

Derivatives of 1,5-Diamino-1*H*-tetrazole: A New Family of Energetic Heterocyclic-Based Salts

Juan Carlos Gálvez-Ruiz,^{†‡} Gerhard Holl,[§] Konstantin Karaghiosoff,[†] Thomas M. Klapötke,^{*,†} Karolin Löhnwitz,[†] Peter Mayer,^{†‡} Heinrich Nöth,^{†‡} Kurt Polborn,^{†‡} Christoph J. Rohbogner,[†] Max Suter,^{†‡} and Jan J. Weigand[†]

Chair of Inorganic Chemistry, Ludwig-Maximilian University of Munich, Butenandtstrasse 5-13 (Haus D), 81377 Munich, Germany, and Bundeswehr Research Institute for Materials, Fuels and Lubricants, Swisttal-Heimerzheim, Grosses Cent, D-53913 Swisttal, Germany

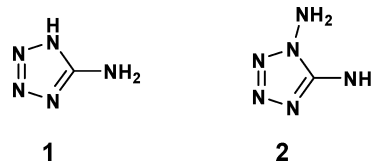
Received January 22, 2005

1,5-Diamino-1*H*-tetrazole (**2**, DAT) can easily be protonated by reaction with strong mineral acids, yielding the poorly investigated 1,5-diaminotetrazolium nitrate (**2a**) and perchlorate (**2b**). A new synthesis for **2** is introduced that avoids lead azide as a hazardous byproduct. The reaction of 1,5-diamino-1*H*-tetrazole with iodomethane (**7a**) followed by the metathesis of the iodide (**7a**) with silver nitrate (**7b**), silver dinitramide (**7c**), or silver azide (**7d**) leads to a new family of heterocyclic-based salts. In all cases, stable salts were obtained and fully characterized by vibrational (IR, Raman) spectroscopy, multinuclear NMR spectroscopy, mass spectrometry, elemental analysis, X-ray structure determination, and initial safety testing (impact and friction sensitivity). Most of the salts exhibit good thermal stabilities, and both the perchlorate (**2b**) and the dinitramide (**7c**) have melting points well below 100 °C, yet high decomposition onsets, defining them as new (**7c**), highly energetic ionic liquids. Preliminary sensitivity testing of the crystalline compounds indicates rather low impact sensitivities for all compounds, the highest being that of the perchlorate (**2b**) and the dinitramide (**7c**) with a value of 7 J. In contrast, the friction sensitivities of the perchlorate (**2b**, 60 N) and the dinitramide (**7c**, 24 N) are relatively high. The enthalpies of combustion ($\Delta_c H^\circ$) of **7b–d** were determined experimentally using oxygen bomb calorimetry: $\Delta_c H^\circ$ (**7b**) = –2456 cal g^{–1}, $\Delta_c H^\circ$ (**7c**) = –2135 cal g^{–1}, and $\Delta_c H^\circ$ (**7d**) = –3594 cal g^{–1}. The standard enthalpies of formation ($\Delta_f H^\circ$) of **7b–d** were obtained on the basis of quantum chemical computations using the G2 (G3) method: $\Delta_f H^\circ$ (**7b**) = 41.7 (41.2) kcal mol^{–1}, $\Delta_f H^\circ$ (**7c**) = 92.1 (91.1) kcal mol^{–1}, and $\Delta_f H^\circ$ (**7d**) = 161.6 (161.5) kcal mol^{–1}. The detonation velocities (*D*) and detonation pressures (*P*) of **2b** and **7b–d** were calculated using the empirical equations of Kamlet and Jacobs: $D(\mathbf{2b}) = 8383 \text{ m s}^{-1}$, $P(\mathbf{2b}) = 32.2 \text{ GPa}$; $D(\mathbf{7b}) = 7682 \text{ m s}^{-1}$, $P(\mathbf{7b}) = 23.4 \text{ GPa}$; $D(\mathbf{7c}) = 8827 \text{ m s}^{-1}$, $P(\mathbf{7c}) = 33.6 \text{ GPa}$; and $D(\mathbf{7d}) = 7405 \text{ m s}^{-1}$, $P(\mathbf{7d}) = 20.8 \text{ GPa}$. For all compounds, a structure determination by single-crystal X-ray diffraction was performed. **2a** and **2b** crystallize in the monoclinic space groups *C2/c* and *P2₁/n*, respectively. The salts of **7** crystallize in the orthorhombic space groups *Pna2₁* (**7a**, **7d**) and *Fdd2* (**7b**). The hydrogen-bonded ring motifs are discussed in the formalism of graph-set analysis of hydrogen-bond patterns and compared in the case of **2a**, **2b**, and **7b**.

Introduction

Aminotetrazoles have the highest content of nitrogen among the organic substances [e.g., 82.3 wt % for 5-amino-1*H*-tetrazole **1** (5-AT) and 84.0 wt % for 1,5-diamino-1*H*-tetrazole **2** (DAT)], and despite their large positive enthalpies

of formation,¹ they exhibit surprisingly high thermal stabilities.^{2–4}



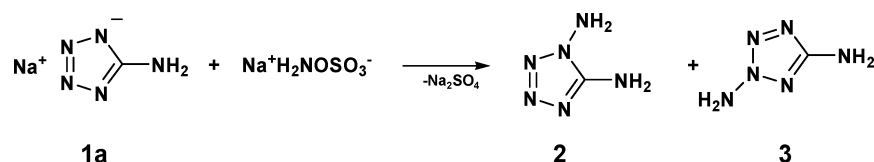
Therefore, aminotetrazoles are prospective materials for the generation of gases, as blowing agents, solid propellants, and other combustible and thermally decomposing systems.

* To whom correspondence should be addressed. E-mail: tmk@cup.uni.muenchen.de. Fax: +49-89-2180-77492. Tel.: +49-89-2180-77491.

[†] Ludwig-Maximilian University Munich.

[‡] X-ray structure analysis.

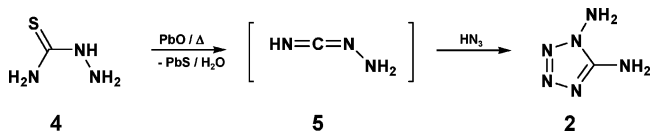
[§] Bundeswehr Research Institute for Materials, Fuels and Lubricants, Swisttal-Heimerzheim.

Scheme 1. Reaction of **1a** with HOSA.

Among the aminotetrazoles, **1** has received by far the most attention in the literature, and it is used as a gas generator and key intermediate in many organic syntheses.⁵ The synthesis of **1** was described as early as in 1892 by Thiele.⁶ Interestingly, **2** and its derivatives had not previously been considered as gas-generating agents, and only little work has been done using **2** as a valuable intermediate in the preparation of high-energy-density materials (HEDMs)^{7,8} or other useful tetrazole-containing compounds.^{9,10} The reason for this might be the difficult accessibility of **2**. Thus far, only three synthetic methods for the preparation of **2** have been described. Through the reaction of **1** as the sodium salt **1a** with hydroxylamine-*O*-sulfonic acid (HOSA), **2** is formed in a low yield (8,5%) together with the 2,5-diamino-2*H*-tetrazole isomer **3** (Scheme 1).¹¹

Gaponik et al.⁹ improved the 1933 reported synthesis of Stolle et al.,¹² who synthesized **2** by reacting thiosemicarbazide (**4**) with lead(II) oxide and sodium azide in a CO₂ atmosphere in ethanol as the solvent. **4** is converted into the corresponding carbodiimide (**5**) with lead(II) oxide, which reacts with in situ formed HN₃ under ring closing to yield derivative **2** (Scheme 2). Unfortunately, this reaction leads to the formation of large amounts of lead azide as the byproduct, which makes this synthesis problematic for an industrial scale.

We are currently investigating the chemistry of tetrazole derivatives with respect to the continuous interest in high-

Scheme 2. Synthesis of **2** According Gaponik et al.⁹

nitrogen compounds as ingredients for propellants and explosives.^{13,14} Among those, the nitrate, dinitramide, and azide salts of nitrogen-rich cations have received major attention for a number of reasons: a high oxygen balance (nitrate and dinitramide salts), a high heat of formation $\Delta_f H^\circ$, the release of large amounts of gases (e.g., N₂) as favored explosion products, and high values of the density ρ . At present, the search for high-energy compounds is mainly directed toward molecular crystals made from neutral molecules. The reason for this is that ionic crystals normally have poor values of $\Delta_f H^\circ_{\text{solid}}$ [solid-state formation enthalpy can be estimated as $\Delta_f H^\circ_{\text{solid}} = \Delta_f H^\circ(\text{gas}) - E_{\text{coh}} - RT$] because of the high contribution of the crystal cohesive energy (E_{coh}). This contribution is comparably small for molecular crystals of covalent compounds, typically lower than 0.12 kcal/g,¹⁵ but for ionic crystals, E_{coh} is typically 1 order of magnitude larger owing to the long-range electrostatic interactions between ions [e.g., low $\Delta_f H^\circ_{\text{solid}}(\text{AN}, \text{ammonium nitrate}) = -1.09$ kcal/g because of the significant cohesion energy of the crystal, $E_{\text{coh}}(\text{AN}) = 2.08$ kcal/g]. To minimize the contribution of E_{coh} , it is important to combine anions (e.g., nitrate, perchlorate, or dinitramide anions for good oxidation abilities) with large cations in order to increase the distance between charged groups. Calculations on ethane and H₃C-NH₃⁺ suggest a very high contribution of the ammonium group -NH₃⁺ to $\Delta_f H^\circ$ (~145 kcal/mol).¹⁶ Thus, some ionic crystals might provide valuable energetic constituents of propellants provided their cohesive energy is not too large. For example, the best known of the highly energetic nitrate and dinitramide salts are the oxidizers ammonium nitrate (AN) and ammonium dinitramide (ADN).^{17,18} In the case of nitrogen-rich anions, we investigated hydrazinium azide¹⁹ and its organic derivatives,²⁰ which are, unfortunately, volatile and hygroscopic and also have relatively low densities.

- (1) Kozyro, A. A.; Simirsky, V. V.; Krasulin, A. P.; Sevruck, V. M.; Kabo, G. J.; Frenkel, M. L.; Gaponik, P. N.; Grigotiev, Yu. V. *Zh. Fiz. Khim.* **1990**, *64*, 656 (in Russian).
- (2) (a) Levchik, S. V.; Balabanovich, A. I.; Ivashkevich, O. A.; Lesnikov, A. I.; Gaponik, P. N.; Costa, L. *Thermochim. Acta* **1992**, *207*, 115; (b) Levchik, S. V.; Balabanovich, A. I.; Ivashkevich, O. A.; Lesnikov, A. I.; Gaponik, P. N.; Costa, L. *Thermochim. Acta* **1993**, *255*, 53; (c) Lesnikov, A. I.; Ivashkevich, O. A.; Levchik, S. V.; Balabanovich, A. I.; Gaponik, P. N.; Kulak, A. A. *Thermochim. Acta* **2002**, *388*, 233.
- (3) Gao, A.; Oyumi, Y.; Brill, T. B. *Combust. Flame* **1991**, *83*, 345.
- (4) Levchik, S. V.; Balabanovich, A. I.; Ivashkevich, O. A.; Gaponik, P. N.; Costa, L. *Polym. Degrad. Stability* **1995**, *47*, 333.
- (5) (a) Neutz, J.; Grosshardt, O.; Schaeufele, S.; Schuppler, H.; Schweikert, W. *Propellants, Explos., Pyrotech.* **2003**, *28* (4), 181; (b) Arai, T.; Kobe, A.; Nagai, N.; Shimizu, S. Japanese Patent, JP 2000302769 A2 20001031, 2000; (c) Rothgery, E. F.; Manke, S. A. U.S. Patent 276,585, 1990; (d) Mayants, A. G.; Pyreseva, K. G.; Gordeichuk, S. S. *Zh. Org. Khim.* **1988**, *24* (4), 884; (e) Demko, Z. P.; Sharpless, K. B. *Org. Lett.* **2002**, *4* (15), 2525; (f) Katritzky, A. R.; Rogovoy, B. V.; Kovalenko, K. V. *J. Org. Chem.* **2003**, *68* (12), 4941; (g) Butler, R. N. In *Comprehensive Heterocyclic Chemistry*, 1st ed.; Potts, K. T., Ed.; Pergamon Press, Oxford, U.K., 1984; Vol. 5, p 791 and references therein.
- (6) Thiele, J. *Liebigs Ann.* **1892**, *270*, 54.
- (7) (a) Xue, H.; Arritt, S. W.; Twamley, B.; Shreeve, J. M. *Inorg. Chem.* **2004**, *43* (25), 7972; (b) Willer, R. L.; Henry, R. A. *J. Org. Chem.* **1988**, *53*, 5371.
- (8) Sinditskii, V. P.; Fogelzang, A. E. *Russ. Khim. Zh.* **1997**, *4*, 74.
- (9) Gaponik, P. N.; Karavai, V. P. *Khim. Geterotsikl. Soedin.* **1984**, 1388.
- (10) Willer, R. L.; Henry, R. A. *J. Org. Chem.* **1988**, *53*(22), 5371.
- (11) Raap, R. *Can. J. Chem.* **1969**, *47* (19), 3677.
- (12) Stollé, R.; Netz, H.; Kramer, O.; Rothschild, S.; Erbe, E.; Schick, O. *J. Prakt. Chem.* **1933**, *138*, 1.

- (13) (a) Chavez, D. E.; Hiskey, M. A. *J. Energ. Mater.* **1999**, *17*, 357; (b) Chavez, D. E.; Hiskey, M. A.; Naud, D. L. *Propellants, Explos., Pyrotech.* **2004**, *29* (4), 209.
- (14) (a) Hammerl, A.; Holl, G.; Kaiser, M.; Klapötke, T. M.; Mayer, P.; Nöth, H.; Piotrowski, H.; Suter, M. *Z. Naturforsch.* **2001**, *56 b*, 857; (b) Hammerl, A.; Holl, G.; Klapötke, T. M.; Mayer, P.; Noth, H.; Piotrowski, H.; Warchhold, M. *Eur. J. Inorg. Chem.* **2002**, *4*, 834; (c) Geith, J.; Klapötke, T. M.; Weigand, J.; Holl, G. *Propellants, Explos., Pyrotech.* **2004**, *29* (1), 3; Klapötke, T. M.; Mayer, P.; Schulz, A.; Weigand, J. *J. Propellants, Explos., Pyrotech.* **2004**, *29* (5), 325.
- (15) Mathieu, D.; Bougrat, P. *Chem. Phys. Lett.* **1999**, *303*, 601.
- (16) (a) Rousseau, E.; Mathieu, D. *J. Comput. Chem.* **2000**, *21*, 367; (b) Audoux, J.; Beaucamp, S.; Mathieu, D.; Poullain, D. In *Proceedings of the 35th International Annual Conference of ICT*; Herrmann, M., Ed.; DWS GmbH: Lichtenau, Germany, 2004; pp 33/1.

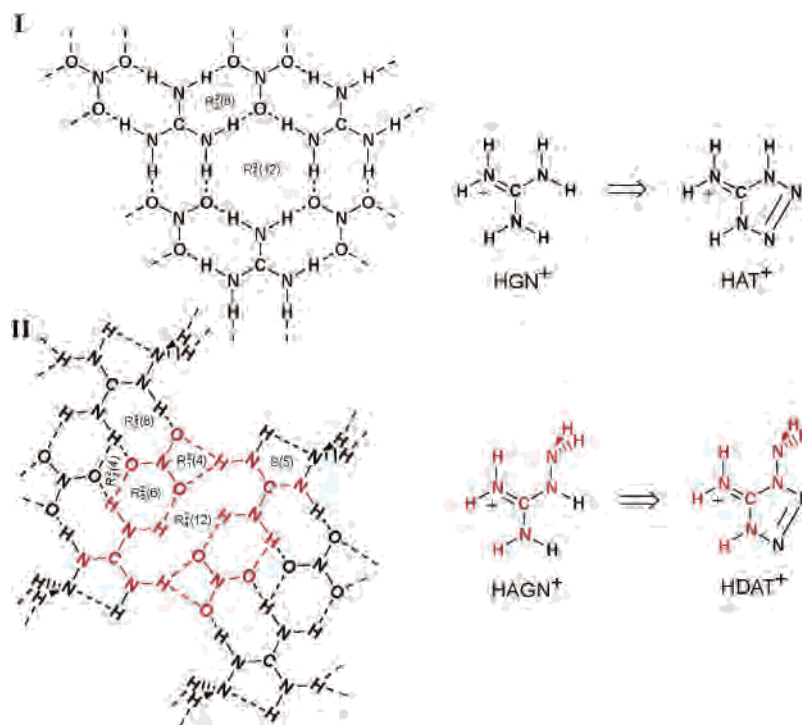


Figure 1. Scheme of the 2D organization pattern of $[\text{HGN}^+\text{NO}_3^-]$ (I) and $[\text{HAGN}^+\text{NO}_3^-]$ (II) through intermolecular hydrogen bonds.

To understand the interplay of cations and anions within a network and to predict important values such as densities, E_{coh} , and $\Delta_f H^\circ$, an algorithm is necessary for predictable and controllable long-range molecular organization.²¹ Basically, the crystal structure of the material is a result of iterative self-assembling of the constituent molecular, co-molecular (bimolecular),²² or ion-pair subunits, considered as fundamental crystal building units. However, the prediction of the solid-state structure of crystals is commonly frustrated by the complexity and lack of directionality of intermolecular forces. The control of packing in three dimensions is elusive owing to the numerous possible intermolecular interactions and multiplicity of structural possibilities. Therefore, it is important to have a closer look into the structural aspects

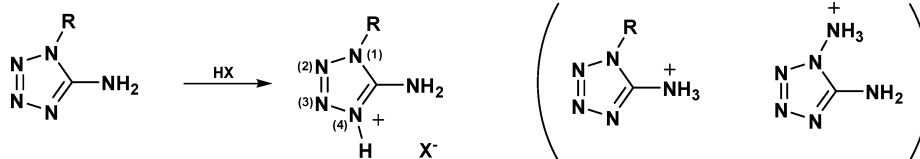
that account for the interplay between such factors as directional demands of the interactions and geometrical dictates the close-packing. In this context, we are also interested in known and new salts of aminotetrazoles, especially with nitrate, dinitramide,²³ and azide as counterions, and we are especially interested in the formation of robust hydrogen-bonded multidimensional networks within these salts. The dimensionality and general structural features of a multidimensional network depend on the modules that serve as “topological directors” and strongly depend on the symmetry of the ions. A search in the Cambridge Structural Database (CSD) revealed that the crystal structure of guanidinium nitrate $[\text{HGN}^+\text{NO}_3^-]$ consists of hydrogen-bonded polar layers, stacked in the third dimension by van der Waals interactions (Figure 1, I).²⁴ The hydrogen-bonded ring motifs, in the formalism of graph-set analysis of hydrogen-bond patterns,²⁵ that are found for $[\text{HGN}^+\text{NO}_3^-]$ are the $R_6^3(12)$ and the very common $R_2^2(8)$ motifs.

As the bond pattern strongly depends on the symmetry of the cations, lowering the symmetry by formally introducing an amino group should modify the hydrogen-bond connectivity pattern. In the case of aminoguanidinium nitrate $[\text{HAGN}^+\text{NO}_3^-]$,²⁶ the terminal NH_2 group is positioned in such a fashion that the hydrogen atoms appear above and below the plane of the rest of the molecule and the lone pair is directed toward the hydrogen atom of one of the $\text{C}=\text{NH}_2$ moieties, forming an intramolecular bond with the motif $S(5)$. The nitrate and aminoguanidinium moieties are approxi-

- (17) (a) Tartakovsky, V. A.; Luk'yanov, O. A. In *Proceedings of the 25th International Annual Conference of ICT*; 1994; pp 13/1. (b) VanSteen, H. H.; Kodde, A. M. *Propellants, Explos., Pyrotech.* **1990**, *15* (2), 58. (c) Patil, D. G.; Jain; Brill, T. B. *Propellants, Explos., Pyrotech.* **1992**, *17* (3), 99. (d) van Niekerk, A. P.; Brower, K. R. *Propellants, Explos., Pyrotech.* **1995**, *20* (5), 273.
- (18) (a) Östmark, H.; Bemm, U.; Langlet, A.; Sandén, R.; Wingborg, N. *J. Energ. Mater.* **2000**, *18*, 123. (b) Venkatachalam, S.; Santhosh, G.; Ninan, K. N. *Propellants, Explos., Pyrotech.* **2004**, *29* (3), 178.
- (19) (a) Klapötke, T. M.; White, P. S.; Tornieporth-Oetting, I. C. *Polyhydron* **1996**, *15*, 2597. (b) Holfter, H.; Klapötke, T. M.; Schulz, A. *Eur. J. Solid State* **1996**, *33*, 855.
- (20) (a) Haberer, T.; Hammerl, A.; Holl, G.; Klapötke, T. M.; Knizek, J.; Nöth, H. *Eur. J. Inorg. Chem.* **1999**, *5*, 849. (b) Haberer, T.; Hammerl, A.; Holl, G.; Klapötke, T. M.; Mayer, P.; Nöth, H. In *Proceedings of the 31th International Annual Conference of ICT*; 2000; pp 150/1. (c) Hammerl, A.; Holl, G.; Hübler, K.; Klapötke, T. M.; Mayer, P. *Eur. J. Inorg. Chem.* **2001**, 755. (d) Hammerl, A.; Holl, G.; Kaiser, M.; Klapötke, T. M.; Mayer, P.; Nöth, H.; Warchhold, M. *Z. Anorg. Allg. Chem.* **2001**, *627*, 1471. (e) Hammerl, A.; Holl, G.; Kaiser, M.; Klapötke, T. M.; Kränzle, R.; Vogt, M. *Z. Anorg. Allg. Chem.* **2002**, *628*, 322.
- (21) Desiraju, G. R. *Crystal Engineering: The Design of Organic Solids*; Elsevier: Amsterdam, 1989.
- (22) Alle, F. H.; Raithby, P. R.; Schields, G. S.; Taylor, R. *Chem. Commun.* **1998**, 1043.

- (23) Klapötke, T. M.; Mayer, P.; Schulz, A.; Weigand, J. J. *J. Am. Chem. Soc.* **2005**, *127*, 2032.
- (24) Katrusiak, A. *Acta Crystallogr.* **1994**, *C50*, 1161.
- (25) (a) Etter, M. C. *Acc. Chem. Res.* **1990**, *23*, 120. (b) Etter, M. C.; MacDonald, J. C. *Acta Crystallogr.* **1990**, *B46*, 256.
- (26) Akella, A.; Keszler, D. *Acta Crystallogr.* **1994**, *C50*, 1974.

Scheme 3

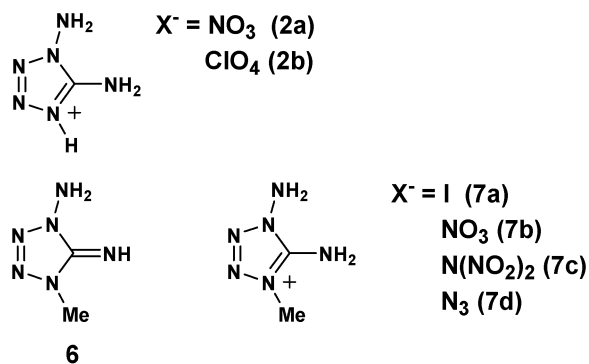


mately coplanar. Within the same plane, the nitrate groups are linked through hydrogen bonds to the N atoms by hydrogen-bonded ring motifs $R_1^2(4)$, $R_2^2(4)$, $R_2^2(6)$, $R_2^2(8)$, and $R_4^2(12)$ (Figure 1, II). Above and below this plane, the groups are bonded intermolecularly through the H atoms of the terminal amino group. In comparison to the above-mentioned salts and in order to gain further details of topological similarities of diaminotetrazolium salts, a closer inspection of the two- and three-dimensional hydrogen-bonded network is discussed in this article.

Aminotetrazoles are heterocycles, rich in electron pairs. Reaction with weak or strong acids leads in the cases of **1** ($R = H$) and **2** ($R = NH_2$) only with strong acids ($X^- = Cl$, Br, I, NO_3 , ClO_4 , SO_4 , picrate)^{9,27} to the formation of the corresponding salts (Scheme 3).

Protonation of **1** and **2** can proceed both on the nitrogen atoms of the tetrazole ring and on the amino group(s). It was determined to proceed unambiguously at the N4 atom of the ring (Scheme 3).²⁸ Nothing is reported in the literature about the isolation of the corresponding azide or dinitramide salts.

In this article, we present our results on the protonation of **2** [**2a** (HNO_3), **2b** ($HClO_4$)] and introduce a new derivative of **2**, the 1-amino-4-methyl-5-imino-4,5-dihydro-1*H*-tetrazole **6**, as its iodide, azide, nitrate, and dinitramide salts (**7a–d**). We also introduce an improved synthesis of **2**, which makes **2** accessible on a larger scale.



Experimental Section

Caution: Silver azide, silver dinitramide, aminotetrazoles, and their derivatives are energetic materials and tend to explode under certain conditions. Appropriate safety precautions should be taken, especially when these compounds are prepared on a larger scale. Laboratories and personnel should be properly grounded, and safety

equipment such as Kevlar gloves, leather coats, face shields, and ear plugs are necessary, especially in the case of **7c**.

All chemical reagents and solvents of analytical grade were obtained from Sigma-Aldrich Fine Chemicals Inc. and used as supplied. MeCN, MeOH, and EtOH were dried according known procedures, freshly distilled, and stored under nitrogen. Silver azide and silver dinitramide²⁹ were prepared according to known procedures. 1H , ^{13}C , and $^{14}N/^{15}N$ NMR spectra were recorded on a JEOL Eclipse 400 instrument. The spectra were measured in DMSO- d_6 or CD_3OD at 25 °C. The chemical shifts are given relative to tetramethylsilane (1H , ^{13}C) or nitromethane ($^{14}N/^{15}N$) as external standards. Coupling constants are given in hertz. Infrared (IR) spectra were recorded on a Perkin-Elmer Spektrum One FT-IR instrument as KBr pellets at 20 °C. Raman spectra were recorded on a Perkin-Elmer Spectrum 2000R NIR FT-Raman instrument equipped with a Nd:YAG laser (1064 nm). The intensities are reported in percent relative to the most intense peak and given in parentheses. Elemental analyses were performed with a Netsch Simultaneous Thermal Analyzer STA 429. Melting points were determined by differential scanning calorimetry (Perkin-Elmer Pyris 6 DSC instrument, calibrated with standard pure indium and zinc). Measurements were performed at a heating rate of $\beta = 10$ °C in closed Al containers with a hole (1 μm) on the top for gas release with a nitrogen flow of 20 mL/min. The reference sample was an Al container with air.

Bomb Calorimetry. For all calorimetric measurements, a Parr 1356 bomb calorimeter (static jacket) equipped with a Parr 207A oxygen bomb for the combustion of highly energetic materials was used.³⁰ The samples (ca. 80–100 mg) were loaded in (energetically) calibrated Parr gelatine capsules (0.9 mL). A Parr 1755 printer was furnished with the Parr 1356 calorimeter to produce a permanent record of all activities within the calorimeter. The experimentally determined values were obtained as the averages of three single measurements each. The calorimeter was calibrated by the combustion of certified benzoic acid in an oxygen atmosphere at a pressure of 3.05 MPa. In case of the perchlorate salts **2b**, the calorimetric experiments were run with additional water. After the experiments, the chlorine concentration was determined according to the Volhard method,³¹ indicating quantitative formation of chloride during the combustion process.

Synthesis of 1,5-Diamino-1*H*-tetrazole (2). A solution of diaminoguanidinium chloride (1.507 g, 12 mmol) in 20 mL of water and 0.5 mL concentrated HCl (37%) was cooled to 0 °C (some solid reprecipitated). With the temperature kept at 0–2 °C, a solution of sodium nitrite (830 mg, 12 mmol) in 5 mL of water was added slowly. The solution obtained was allowed to stand in ice–water for 30 min. It was then brought to pH 8 with solid sodium carbonate, stirred for 20 min at 40 °C, and subsequently evaporated to dryness under vacuum (water aspirator) in a stream of pure

(27) Drake, G.; Hawkins, T. Presented at the AFRL/PRSP AFOSR Ionic Liquids Workshop, Tampa, FL, Mar 2004.

(28) Matulis, V. E.; Lyakhov, A. S.; Gaponik, P. N.; Voitekhovich, S. V.; Ivashkevich, O. A. *J. Mol. Struct.* **2003**, *649*, 309.

(29) How-Ghee, A.; Fraenk, W.; Karaghiosoff, K.; Klapötke, T. M.; Mayer, P.; Nöth, H.; Sprott, J.; Warchhold, M. *Z. Anorg. Allg. Chem.* **2002**, *628*, 2894.

(30) <http://www.parrinst.com/>.

(31) Ohlweiler, O. A.; Meditsch, J. de O.; Kuperstein, S. *Anais Assoc. Bras. Quim.* **1959**, *18*, 17.

nitrogen. The residue was extracted with hot EtOH (3 × 15 mL), leaving, after evaporation, pure 1,5-diamino-1H-tetrazole, which was recrystallized from water (700 mg, 7 mmol, 58%). mp 185–187 °C; IR (KBr, cm⁻¹) $\tilde{\nu}$ = 3324 (vs), 3237 (s), 3154 (s), 1656 (vs), 1632 (sh), 1576 (m), 1329 (s), 1134 (vw), 1109 (m), 1076 (m), 1001 (m), 932 (m), 788 (vw), 745 (w), 699 (w), 686 (m), 626 (sh), 603 (m), 487 (vw); Raman (200 mW, 25 °C, cm⁻¹) $\tilde{\nu}$ = 3323 (12), 3244 (11), 3154 (9), 1670 (9), 1623 (5), 1547 (19), 1496 (5), 1329 (14), 1307 (18), 1133 (3), 1106 (14), 1978 (11), 1001 (5), 951 (4), 792 (100), 698 (15), 323 (24), 231 (13), 140 (18); ¹H NMR (DMSO-*d*₆) δ 6.35 (s, NH₂), 6.40 (s, NH₂); ¹³C NMR (DMSO-*d*₆, 25 °C) δ 155.0; ¹⁵N NMR (DMSO-*d*₆, 25 °C) δ -5.5 (N3), -20.8 (N2), -97.5 (N4), -167.8 (N1-NH₂), -315.2 (N1-NH₂), ¹J_{NH} = 74.6 Hz, -338.3 (C-NH₂), ¹J_{NH} = 87.9 Hz; MS (DEI, 70 eV, >5%) *m/z* (%) 101 (1) [M⁺ + 1], 100 (9) [M⁺], 75 (2), 56 (2), 44 (6), 43 (100), 42 (11), 41 (3), 32 (4), 31 (3), 30 (23), 29 (16), 28 (24), 27 (11), 26 (1), 18 (5), 17 (5), 16 (5), 13 (1); CH₄N₆ (100.08) calcd C 12.0, H 4.0, N 84.0%; found C 12.1, H 3.9, N 83.7%.

Synthesis of 1,5-Diamino-1H-tetrazolium Nitrate (2a). Method 1. **2** (1000.8 mg, 10 mmol) and 1.4 mL of concentrated HNO₃ (65%) were gently heated to give a clear solution. Upon careful addition of Et₂O (20 mL) to this solution, the product separated as a white precipitate. The precipitate was filtered and washed several times with Et₂O to give **2a** (1.50 g, 9.2 mmol, 92%). Recrystallization from EtOH/H₂O yielded **2a** as colorless plates.

Method 2. **2** (20 g, 0.2 mol) was dissolved at 70 °C in a solution of 35 mL of concentrated HNO₃ (65%) and 20 mL of H₂O. After being cooled to room temperature, the solution was left at 5 °C for crystallization. After filtration, the product was washed with cold EtOH and dried in vacuo over P₄O₁₀ (30.5 g, 18.7 mmol, 93%). mp 138–139 °C; IR (KBr, cm⁻¹) $\tilde{\nu}$ = 3425 (s), 3341 (s), 3146 (w), 2961 (w), 2841 (w), 2806 (vw), 2659 (w), 2472 (vw), 2346 (vw), 1726 (s), 1649 (vw), 1609 (w), 1494 (m), 1436 (w), 1384 (vs, NO₃⁻), 1305 (s), 1107 (m), 1039 (s), 976 (m), 841 (m), 728 (w), 710 (m), 660 (vw), 475 (m); Raman (200 mW, 25 °C, cm⁻¹) $\tilde{\nu}$ = 3342 (6), 2997 (1), 1735 (1), 1567 (13), 1488 (7), 1465 (8), 1400 (4), 1342 (9), 1092 (7), 1057 (30), 1042 (100, NO₃⁻), 745 (57), 730 (9), 718 (9), 401 (13), 151 (18), 136 (11), 119 (9); ¹H NMR (CD₃OD) δ 5.14 (s, -NH, NH₂); ¹³C NMR (CD₃OD, 25 °C) δ 151.2; ¹⁴N NMR (CD₃OD, 25 °C) δ -11.6 (NO₃⁻), -27.0 (N3, N2, $\Delta\nu_{1/2}$ = 1503 Hz), -164 (N1-NH₂, N4-H, $\Delta\nu_{1/2}$ = 1271 Hz), -343 (N1-NH₂, C-NH₂ $\Delta\nu_{1/2}$ = 1329 Hz); ¹⁵N NMR (CD₃OD, 25 °C) δ -11.6 (NO₃⁻), -21.9 (N3), -33.1 (N2), -164.8 (N1-NH₂), -170.4 (N4-H), -319.6 (N1-NH₂), 333.3 (C-NH₂); *m/z* (FAB⁺, xenon, 6 keV, m-NBA matrix) 101 [DAT + H]⁺; *m/z* (DEI) 100 [(M - HNO₃) (9)], 45 (21), 44 (5), 43 (100), 42 (11), 41 (4), 30 (22), 29 (15), 28 (25), 27 (9); CH₅N₇O₃ (163.10) calcd C 7.4, H 3.1, N 60.1%; found C 7.3, H 3.1, N 59.8%.

Synthesis of 1,5-Diamino-1H-tetrazolium Perchlorate (2b). Method 1. DAT (**2**; 1000.8 mg, 10 mmol) and 502 μ L of HClO₄ (70%) were gently heated to give a clear solution. This solution was washed five times with Et₂O (10 mL). The resulting aqueous phase was overlaid with Et₂O (20 mL) and left for crystallization. After 1 week, the perchlorate **2b** starts to crystallize as large colorless plates (1.90 g, 9.5 mmol, 95%).

Method 2. A Schlenk flask was loaded with **2** (1000.8 mg, 10 mmol), and dry methanol (15 mL) was added via a syringe. Concentrated perchloric acid (837 mg, 10 mmol, 70%) was carefully added. The colorless homogeneous reaction mixture was stirred for 1 h at ambient temperature. High-quality crystals were formed from the concentrated methanol solution layered with diethyl ether (1.85 g, 9.3 mmol, 93%). mp 97–98 °C; IR (KBr, cm⁻¹) $\tilde{\nu}$ = 3416 (s), 3319 (s), 3151 (s), 3094 (s), 1718 (vs), 1616 (m), 1563 (w), 1509

(vw), 1338 (m), 1290 (m), 1145 (vs), 1109 (vs), 1090 (vs), 1013 (m), 941 (m), 781 (vw), 756 (m), 703 (m), 688 (m), 653 (m), 636 (s), 627 (s), 572 (m); Raman (200 mW, 25 °C, cm⁻¹) $\tilde{\nu}$ = 3295 (4), 3219 (3), 1725 (4), 1637 (6), 1585 (3), 1512 (6), 1445 (7), 1316 (19), 1134 (8), 1076 (7), 1036 (7), 1004 (6), 926 (100), 785 (64), 689 (9), 626 (18), 462 (27) 456 (27), 305 (22), 257 (7), 141 (15); ¹H NMR (CD₃OD, 25 °C) δ 5.21 (s, -NH, NH₂); ¹³C NMR (CD₃OD, 25 °C) δ 149.7; ¹⁴N NMR (CD₃OD, 25 °C) δ -30 (N3, N2, $\Delta\nu_{1/2}$ = 1936 Hz), -179 (N1-NH₂, N4-H, $\Delta\nu_{1/2}$ = 1329 Hz), -346 (N1-NH₂, C-NH₂ $\Delta\nu_{1/2}$ = 1214 Hz); ¹⁵N NMR (CD₃OD, 25 °C) δ -20.5 (N3), -36.6 (N2), -169.4 (N1-NH₂), -177.5 (N4-H), -317.9 (N1-NH₂), 329.6 (C-NH₂); ³⁵Cl NMR (CD₃OD) δ 1.01 (s, ClO₄⁻); *m/z* (FAB⁺, xenon, 6 keV, m-NBA matrix) 101 [DAT + H]⁺; CH₅N₆ClO₄ (200.54) calcd C 5.6, H 2.5, N 41.9%; found C 5.9, H 2.8, N 41.5%.

Synthesis of 1,5-Diamino-4-methyl-1H-tetrazolium Iodide (7a). To a solution of **2** (1.50 g, 15 mmol) in 50 mL of MeCN was added an excess of MeI (6.4 mL, 90 mmol), and the resulting mixture was refluxed for 14 h. The color of the reaction mixture turned from colorless to deep red. Colorless crystals started to separate from the cold solution after 5 days (750 mg, 20%). Another crop of the product was obtained by evaporation of the mother liquor in vacuo to one-half its initial volume (2.4 g, 66%); total yield (86%). IR (KBr, cm⁻¹) $\tilde{\nu}$ = 3215 (s), 3068 (s), 1702 (vs), 1613 (m), 1571 (w), 1445 (w), 1426 (w), 1392 (m), 1368 (w), 1245 (w), 1197 (w), 1117 (w), 1031 (m), 1001 (w), 913 (vw), 787 (w), 773 (w), 707 (vw), 671 (vw), 634 (w), 606 (w), 586 (m), 528 (w); Raman (200 mW, 25 °C, cm⁻¹) $\tilde{\nu}$ = 3243 (19), 3168 (20), 3020 (7), 2940 (25), 1700 (6), 1613 (6), 1572 (7), 1524 (6), 1445 (5), 1424 (5), 1390 (11), 1369 (24), 1190 (5), 1116 (6), 1025 (13), 998 (4), 788 (64), 602 (15), 545 (5), 412 (6), 308 (9), 292 (11), 275 (7), 182 (11); ¹H NMR (DMSO-*d*₆, 25 °C) δ 3.84 (s, CH₃), 7.01 (s, C-NH₂), 8.97 (s, N-NH₂); ¹³C NMR (DMSO-*d*₆, 25 °C) δ 39.9 (CH₃), 148.0 (C); ¹⁵N NMR (DMSO-*d*₆, 25 °C) δ -24.2 (N3), -35.5 (N2), -167.8 (N1-NH₂), -215.6 (N4-Me), -309.1 (N1-NH₂), 320.0 (C-NH₂); *m/z* (FAB⁺, xenon, 6 keV, m-NBA matrix) 115 [MeDAT]⁺; C₂H₇IN₆ (242.02) calcd C 9.9, H 2.9, N 34.7%; found C 9.8, H 2.9, N 34.8%.

Synthesis of 1,5-Diamino-4-methyl-1H-tetrazolium Nitrate (7b). To a solution of **7a** (1.21 g, 5 mmol) in 15 mL of MeOH/MeCN (1:1) was added AgNO₃ (0.85 g, 5 mmol), and the resulting mixture was stirred for 30 min in the dark. After removal of AgI, the solvents were evaporated in vacuo, and the residue was recrystallized from MeOH/Et₂O (728 mg, 4.7 mmol, 93%). mp 121–122 °C; IR (KBr, cm⁻¹) $\tilde{\nu}$ = 3406 (vw), 3256 (w), 3216 (m), 3045 (s), 1699 (vs), 1614 (m), 1584 (vw), 1384 (vs, -NO₃⁻), 1356 (vw), 1261 (w), 1198 (w), 1115 (w), 1036 (m), 1006 (w), 911 (m), 832 (w), 787 (vw), 774 (m), 670 (w), 635 (w), 605 (w), 579 (m), 525 (w); Raman (200 mW, 25 °C, cm⁻¹) $\tilde{\nu}$ = 3312 (5), 3208 (5), 3046 (4), 2965 (12), 1705 (2), 1634 (4), 1607 (3), 1531 (5), 1459 (5), 1376 (19), 1250 (2), 1122 (4), 1049 (100), 985 (3), 871 (1), 793 (69), 721 (7), 609 (17), 326 (10), 304 (6), 193 (7), 131 (7); ¹H NMR (CD₃OD, 25 °C) δ 3.92 (s, CH₃), 4.87 (s, C-NH₂, N-NH₂); ¹³C NMR (CD₃OD, 25 °C) δ 33.6 (CH₃), 148.1 (C); ¹⁴N NMR (CD₃OD, 25 °C) δ -33.0 (N2, N3, $\Delta\nu_{1/2}$ = 1600 Hz), -190.6 (N1-NH₂, $\Delta\nu_{1/2}$ = 1480 Hz) -334.0 (N1-NH₂, C-NH₂ $\Delta\nu_{1/2}$ = 910 Hz); *m/z* (FAB⁺, xenon, 6 keV, m-NBA matrix) 115 [MeDAT]⁺; *m/z* (FAB⁻, xenon, 6 keV, m-NBA matrix) 62 [NO₃]⁻; C₂H₇N₇O₃ (177.15): calcd C 13.6, H 4.0, N 55.4%; found C 13.4, H 3.8, N 55.1%.

Synthesis of 1,5-Diamino-4-methyl-1H-tetrazolium Dinitramide (7c). To a solution of **7a** (1.21 g, 5 mmol) in 20 mL of MeCN under N₂ was added a solution of AgN(NO₂)₂ in 15 mL of MeCN

Table 1. Crystal Data and Details of the Structure Determination for Compounds **2a**, **2b**, and **7a–d**

	2a	2b	7a	7b	7c^d	7d
formula	CH ₅ N ₆ ⁺ NO ₃ ⁻	CH ₅ N ₆ ⁺ ClO ₄ ⁻	C ₂ H ₇ N ₆ ⁺ I ⁻	C ₂ H ₇ N ₆ ⁺ NO ₃ ⁻	C ₂ H ₇ N ₆ ⁺ N(NO ₂) ₂ ⁻	C ₂ H ₇ N ₆ ⁺ N ₃ ⁻
formula weight (g mol ⁻¹)	163.12	200.56	227.12	177.15	221.17	157.17
crystal system	monoclinic	monoclinic	orthorhombic	orthorhombic	orthorhombic	orthorhombic
space group	<i>C2/c</i>	<i>P2_{1/n}</i>	<i>Pna2₁</i>	<i>Fdd2</i>	<i>P2₁2₁2₁</i>	<i>Pna2₁</i>
<i>a</i> (Å)	17.898(3)	9.063(3)	8.9104(9)	18.547(2)	5.2632(2)	7.815(2)
<i>b</i> (Å)	5.2292(8)	5.013(1)	16.506(2)	30.709(3)	12.3766(5)	17.913(4)
<i>c</i> (Å)	14.479(2)	15.659(4)	5.4554(6)	5.4881(4)	13.1225(6)	5.262(1)
β (deg)	112.23(1)	100.022(5)	90	90	90	90
<i>V</i> (Å ³)	1254.5(3)	700.5(4)	802.35(2)	3125.8(5)	854.81(6)	735.7(3)
<i>Z</i>	8	4	4	4	4	4
ρ_{calcd} (g/cm ⁻³)	1.727	1.902	1.880	1.506	1.719	1.417
μ (mm ⁻¹)	0.159	0.537	3.910	0.134	0.156	0.111
λ (Mo K α) (Å)	0.71073	0.71073	0.71073	0.71073	0.71073	0.71073
<i>T</i> (K)	293(2)	193(2)	200(2)	213(2)	200(2)	200(2)
reflns collected	1027	3744	4473	4017	8108	6387
independent reflns	981	1447	1612	1230	1513	1157
<i>R</i> _{int}	0.015	0.0731	0.0549	0.0861	0.067	0.1045
obsd reflns	900	1225	1104	983	1192	705
<i>F</i> (000)	672	408	452	1472	456	328
<i>R</i> ₁ ^a	0.0346	0.0466	0.0488	0.0587	0.0363	0.1172
w <i>R</i> ₂ ^b	0.0861	0.1061	0.0740	0.1176	0.0888	0.1290
weighting scheme ^c	0.0446, 1.452	0.0598, 0.1484	0.0430, 0.000	0.0736, 0.000	0.0510, 0.000	0.0504, 0.000
GOF	1.050	1.068	0.868	1.050	1.020	0.976
no. parameters	101	129	93	137	166	118
CCDC	261253	261252	261254	261255	258034	261459

^a $R_1 = \sum ||F_o| - |F_c|| / \sum |F_o|$. ^b $R_w = [\sum (F_o^2 - F_c^2) / \sum (F_o^2)]^{1/2}$. ^c $w = [\sigma_c^2(F_o^2) + (xP)^2 + yP]^{-1}$, $P = (F_o^2 - 2F_c^2)/3$. ^d From ref 23.

(1070 mg, 5 mmol).²⁸ After 1 h, the precipitated AgI was removed by filtration, and the solution was concentrated to one-half its initial volume. The solution was layered with Et₂O and kept in a refrigerator. Crystals deposit in the course of 1 week (940 mg, 4.3 mmol, 85%). mp 85–86 °C; IR (KBr, cm⁻¹) $\tilde{\nu}$ = 3335 (s), 3282 (s), 3245 (s), 3198 (s), 3141 (s), 1709 (vs), 1632 (m), 1592 (w), 1526 (vs), 1422 (vs), 1374 (m), 1322 (m), 1170 (vs, br), 1018 (vs), 961 (m), 944 (m), 819 (m), 791 (m), 780 (m), 764 (m), 738 (m), 705 (m), 665 (vw), 603 (m), 581 (m), 523 (w); Raman (200 mW, 25 °C, cm⁻¹) $\tilde{\nu}$ = 3334 (9), 3284 (11), 3227 (10), 3047 (4), 2966 (12), 1708 (5), 1633 (7), 1589 (6), 1526 (9), 1402 (14), 1375 (23), 1322 (65), 1252 (4), 1165 (6), 1123 (7), 1049 (35), 1018 (12), 946 (10), 822 (36), 792 (100), 764 (8), 721 (3), 602 (20), 483 (21), 456 (7), 302 (22), 276 (12), 132 (21); ¹H NMR (CD₃OD, 25 °C) δ 3.91 (s, CH₃), 4.82 (s, C–NH₂, N–NH₂); ¹³C NMR (CD₃OD, 25 °C) δ 34.9 (CH₃), 149.3 (C); ¹⁴N NMR (CD₃OD, 25 °C) δ –12.4 (N(NO₂)₂⁻, $\Delta\nu_{1/2}$ = 60 Hz), –60.4 (N₃, N₂, $\Delta\nu_{1/2}$ = 850 Hz), –189.9 (N1–NH₂, N4–Me, N(NO₂)₂⁻, $\Delta\nu_{1/2}$ = 1120 Hz), –334.0 (N1–NH₂, C–NH₂, $\Delta\nu_{1/2}$ = 950 Hz); *m/z* (FAB⁺, xenon, 6 keV, m-NBA matrix) 115 [MeDAT]⁺; *m/z* (FAB⁻, xenon, 6 keV, m-NBA matrix) 106 [N(NO₂)₂]⁻; C₂H₇N₉O₄ (221.14) calcd C 10.9, H 3.2, N 57.0%; found C 11.1, H 3.3, N 56.4%.

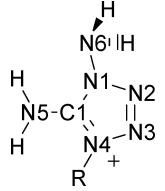
Synthesis of 1,5-Diamino-4-methyl-1H-tetrazolium Azide (**7d**).

To a solution of **7a** (1.21 g, 5 mmol) in 30 mL of H₂O was added an excess of AgN₃ (1.125 g, 7.5 mmol), and the resulting mixture was stirred for 24 h in the dark. After the excess AgN₃ and AgI had been removed, the water was evaporated in vacuo, and the residue recrystallized from EtOH/Et₂O (616 mg, 4 mmol, 90%). mp 135–137 °C (decomp); IR (KBr, cm⁻¹) $\tilde{\nu}$ = 3264 (s, br), 3118 (s, br), 2939 (s, br), 2036 (vs), 1705 (vs), 1626 (s), 1454 (w), 1422 (w), 1395 (m), 1372 (w), 1345 (w), 1245 (w), 1191 (w), 1120 (w), 1033 (w), 1004 (w), 911 (vw), 792 (m), 734 (vw), 683 (s), 628 (m), 601 (w), 534 (w), 467 (w); Raman (200 mW, 25 °C, cm⁻¹) $\tilde{\nu}$ = 3251 (11), 3173 (15), 3012 (9), 2950 (24), 1708 (15), 1604 (17), 1525 (16), 1426 (16), 1395 (21), 1375 (33), 1340 (33), 1250 (17), 1194 (11), 1122 (14), 1031 (14), 871 (1), 793 (100), 630 (11), 606 (28), 343 (27), 306 (14), 280 (14), 180 (64); ¹H NMR (DMSO-*d*₆, 25 °C) δ 3.77 (s, CH₃), 4.81 (s, C–NH₂), 6.82 (s, N–NH₂); ¹³C NMR (DMSO-*d*₆, 25 °C) δ 33.8 (CH₃), 147.5 (C); ¹⁴N NMR

(DMSO-*d*₆, 25 °C) δ –133.2 (N_β, $\Delta\nu_{1/2}$ = 120 Hz), –277.6 (N_α, $\Delta\nu_{1/2}$ = 320 Hz); ¹⁵N NMR (CD₃OD, 25 °C) δ –23.5 (N₃), –34.7 (N₂), –134.4 (N_β), –169.2 (N1–NH₂), –187.4 (N4–H), –282.8 (N_α), –323.7 (N1–NH₂), 331.2 (C–NH₂); *m/z* (FAB⁺, xenon, 6 keV, m-NBA matrix) 115 [MeDAT]⁺; *m/z* (FAB⁻, xenon, 6 keV, m-NBA matrix) 42 [N₃]⁻; C₂H₇N₉ (157.17) calcd C 15.2, H 4.5, N 80.2%; found C 15.0, H 4.5, N 80.1%.

X-ray Analyses. Crystals were obtained as described above. X-ray-quality crystals of **2a** (CCDC 261253) were mounted in a Pyrex capillary, and the X-ray crystallographic data were collected on a Nonius Mach3 diffractometer with graphite-monochromated Mo K α radiation (λ = 0.71073 Å). The X-ray crystallographic data for **2b** (CCDC 261252), **7a** (CCDC 261254), and **7b** (CCDC 261255) were collected on a Siemens P4 diffractometer equipped with a Siemens CCD area detector, and for **7d** (CCDC 261459) the data were collected on an Enraf-Nonius Kappa CCD diffractometer using graphite-monochromated Mo K α radiation (λ = 0.71073 Å). Unit cell parameters for **2a** were obtained by setting angles of a minimum of 25 carefully centered reflections having $2\theta > 20^\circ$; the choice of the space group was based on systematically absent reflections and confirmed by the successful solution and refinements of the structures. The structures were solved by direct methods (SHELXS-86, SHELXS-97)^{32a,b} and refined by means of full-matrix least-squares procedures using SHELXL-93 and SHELXL-97. Empirical absorption correction by Ψ scans was used for **2b**. In the cases of **2b**, **7a**, and **7b**, numerical absorption correction was performed using SADABS, and for **7d**, XRed was used.^{32c,d} Crystallographic data are summarized in Table 1. Selected bond lengths and angles are reported in Table 2. All non-hydrogen atoms were refined anisotropically. In the case of **2a**, the hydrogen atoms were included at geometrically idealized positions and refined. They were assigned fixed isotropic temperature factors with the value of 1.2*B*_{eq} of the atom to which they were bonded. The hydrogen

- (32) (a) Sheldrick, G. M. *SHELXL-86, Program for Solution of Crystal Structures*; University of Göttingen: Göttingen, Germany, 1986. (b) Sheldrick, G. M. *SHELXL-97, Program for Solution of Crystal Structures*; University of Göttingen: Göttingen, Germany, 1997. (c) Gabe, E. J.; Le Page, Y.; Charland, J. P.; Lee, F. L.; White, P. S. *J. Appl. Crystallogr.* **1989**, *22*, 384. (d) *XRed*, rev. 1.09; STOE & Cie GmbH: Darmstadt, Germany, 1997.

Table 2. Comparison of Selected Interatomic Distances (Å) and Bond Angles (deg) of **2**, **2a**, **2b**, and **7a–d**


	2 ^a	2a R = H	2b R = H	7a R = C2	7b R = C2	7c ^b R = C2	7d R = C2
Bond Lengths							
N1–C1	1.345(1)	1.323(9)	1.340(3)	1.355(1)	1.340(4)	1.335(3)	1.328(6)
N1–N2	1.363(1)	1.366(2)	1.368(2)	1.383(9)	1.364(4)	1.361(3)	1.373(6)
N2–N3	1.279(1)	1.260(4)	1.272(3)	1.234(9)	1.280(4)	1.274(3)	1.275(6)
N3–N4	1.367(1)	1.354(8)	1.361(3)	1.386(8)	1.354(4)	1.361(3)	1.362(6)
N1–N6	1.383(1)	1.385(2)	1.387(2)	1.378(9)	1.388(3)	1.402(3)	1.390(5)
C1–N4	1.327(1)	1.336(3)	1.333(3)	1.339(8)	1.341(3)	1.336(3)	1.321(6)
C1–N5	1.334(1)	1.302(4)	1.304(3)	1.32(1)	1.299(4)	1.315(3)	1.321(7)
N4–R	–	–	–	1.42(1)	1.458(4)	1.445(3)	1.470(6)
Bond Angles							
C1–N1–N2	108.84(8)	110.4(2)	110.4(2)	108.3(7)	110.4(2)	110.1(2)	109.8(4)
N2–N1–N6	125.13(8)	124.5(1)	126.0(2)	125.7(6)	126.1(2)	124.3(2)	125.7(4)
N5–C1–N1	123.87(9)	130.3(2)	127.1(2)	125.7(6)	127.3(3)	127.3(2)	126.0(5)
C1–N4–N3	105.56(8)	110.0(2)	110.6(2)	108.2(7)	110.0(2)	110.0(2)	110.2(4)
N3–N2–N1	105.79(8)	107.2(1)	107.4(2)	108.6(6)	107.1(2)	107.8(2)	107.2(4)
C1–N1–N6	126.02(9)	125.1(1)	123.5(2)	125.8(6)	123.4(3)	125.6(2)	124.4(4)
N5–C1–N4	128.17(8)	130.3(2)	129.2(2)	129.1(7)	128.7(3)	128.5(2)	129.2(5)
N4–C1–N1	107.90(8)	103.7(1)	103.7(2)	105.2(9)	103.9(2)	104.2(2)	104.9(5)
N2–N3–N4	111.92(9)	108.7(1)	108.0(2)	109.6(6)	108.5(2)	107.9(2)	107.9(4)
C1–N4–R	–	–	–	128.5(7)	128.2(3)	127.7(2)	128.8(4)

^a From ref 44. ^b From ref 23.

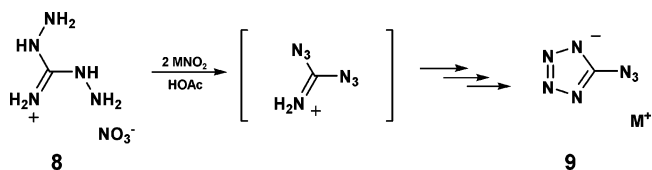
atoms of compound **2b**, **7a**, **7b**, and **7d** were located from difference electron-density map and refined isotropically. In the cases of **7a** and **7d**, the hydrogen atoms of the methyl group were inserted in idealized positions and were refined riding on the atom to which they were bonded (fixed isotropic temperature factors with the value of 1.2*B*_{eq}). Further information on the crystal-structure determinations (excluding structure factors) has been deposited with the Cambridge Crystallographic Data Centre as supplementary publication nos. 261252, 261253, 261254, 261255, and 261459. Copies of the data can be obtained free of charge on application to CCDC, 12 Union Road, Cambridge CB2 1EZ, U.K. [fax (+44) 1223-336-033, e-mail deposit@ccdc.cam.ac.uk]. Crystallographic data in CIF format are also available as Supporting Information.

Results and Discussion

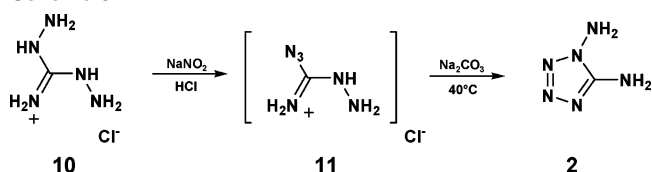
Synthesis. The synthesis strategy for **2** is based on the studies of Lieber et al. who treated diaminoguanidine nitrate (**8**) with 1 and 2 equiv of nitrous acid in a buffered acetic acid media.³³ According to Lieber, the treatment of **8** with 2 equiv of nitrous acid (NaNO₂ or KNO₂ in acetic solution), yielded the corresponding alkali metal salt of tetrazolyl azide (**9**) as the only isolable product.³⁴

The reaction with 1 equiv of nitrous acid in acetic acid media resulted mainly in the recovery of **8** (80–95%) and the isolation of a small quantity of the corresponding metal salt of tetrazolyl azide **9** (Scheme 4). It is known that the reaction of nitrous acid with aminoguanidine is strongly dependent on the reaction conditions and that aminoguanidine reacts with nitrous acid in three ways: If the reaction is carried out in strong mineral acids, it leads to the formation

Scheme 4. Reaction of **8** with Nitrous Acid in Buffered Acetic Acid Media



Scheme 5



of guanyl azide. In aqueous solution alone, 1-guanyl-4-nitroso-aminoguanilyltetrazene is formed, whereas in a solution of acetic acid, ditetrazolyltriazene is obtained.³⁵ In general, the reaction between HNO₂ and a hydrazine moiety can yield the corresponding azide or result in the degradation of the hydrazine to the corresponding amine depending on the pH.³⁶ On this basis, we modified the reaction conditions and used diaminoguanidinium chloride (**10**) in hydrochloric acid as the starting material. After diazotation, the reaction mixture was carefully brought to pH 8 with sodium carbonate to deprotonate the intermediately formed amino-substituted azido guanyl chloride **11**. **11** cyclizes under these reaction conditions, and **2** is formed in an overall yield of 58% (Scheme 5).

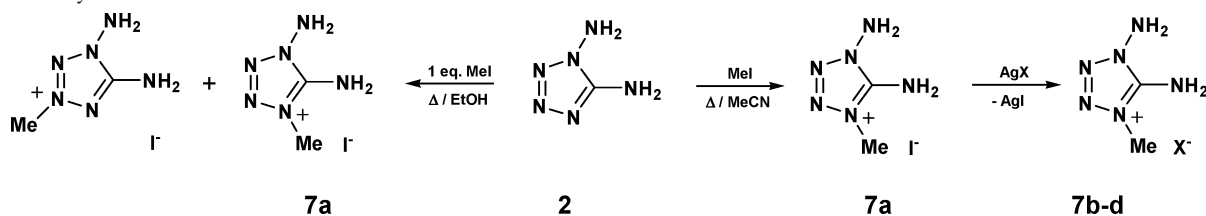
The preparation of **2a** and **2b** was easily archived by the reaction of **2** with the corresponding acids (see Experimental

(33) Lieber, E.; Levering, D. R. *J. Am. Chem. Soc.* **1951**, *73*, 1313.

(34) Hammerl, A.; Klapötke, T. M.; Nöth, H.; Warchold, M. *Propellants, Explos., Pyrotech.* **2003**, *28* (4), 174.

(35) Lieber, E.; Smith, G. B. L. *Chem. Rev.* **1939**, *25*, 213.

(36) Perrott, J. R.; Stedman, G.; Uysal, N. *Dalton Trans.* **1976**, *20*, 2058.

Scheme 6. Synthesis of **7a** and Methathesis to **7b–d**.

Section; **2a** 93%, **2b** 97% yield). All attempts to prepare a corresponding HDAT⁺N₃[−] species were unsuccessful because of the low acidity of HN₃. It is known from other authors that, in high-nitrogen heterocyclic rings having amino groups attached to the ring, there is an electronic interaction between the amino groups and the ring system. As a consequence, a significant reduction of the basicity of the lone pair of the amino group is observed (e.g., 4-amino-1,2,4-triazole has a pK_a of 2.25,³⁷ and 1*H*-1,2,4-triazole has a pK_a of 10.04,³⁸ whereas 1*H*-1,2,3-triazole has a pK_a of 8.2³⁶). We prepared 1,5-diamino-4-methyl-1*H*-tetrazolium iodide (**7a**) via the protonation of **2** with iodomethane. Because of the formal exchange of the proton at N4 by a methyl group, we expected a lower acidity and hence a higher stability of the corresponding azide. The reaction of **2** with MeI is regiospecific when performed in refluxing acetonitrile using an excess of MeI. It yields **7a** in an overall yield of 86%. The reaction of **2** with 1 equiv of MeI in refluxing EtOH yields a mixture of isomers that could not easily be separated. By methathesis of **7a** with the corresponding silver salts, the nitrate (**7b**, X = NO₃, 93%), dinitramide [**7c**, X = N(NO₂)₂, 85%], and azide (**7d**, X = N₃, 90%) were obtained (Scheme 6). All salts were formed in good to excellent yields in high purity and could be recrystallized from concentrated alcoholic solutions layered with diethyl ether. Compared to the low-melting-point salts of 1,2,4- and 1,2,3-triazole systems, introduced by Drake et al.,³⁹ two of our new salts can also be classified as ionic liquids,⁴⁰ namely, **2b** (mp 97 °C) and **7c** (mp 85 °C); the melting points of the others lies an average of 40 °C higher (see Table 6 below).

Vibrational spectroscopy was useful in qualitative analysis of all of the salts, especially in evaluating the formation of the hydrogen-bond network. In all spectra, the bands of the respective energetic anions (N₃[−], ClO₄[−], NO₃[−] and N(NO₂)₂[−]) were obvious, and as these bands usually have characteristic fingerprints in both the infrared and the Raman spectra, they could be identified easily. The nitrate anion, NO₃[−], usually has a strong stretch at 1345 cm^{−1} in the infrared spectrum and a strong band around 1043–1050 cm^{−1} in the Raman spectrum.⁴¹ The perchlorate anion, ClO₄[−], has a strong broad stretch centered around 1119 cm^{−1} in the infrared spectra,

and strong bands at 958 and 459 cm^{−1} in the Raman spectrum.⁴² The dinitramine anion, N(NO₂)₂[−], has strong stretches in the infrared spectrum at around 1530, 1445, 1345, 1183, and 1025 cm^{−1} and strong bands in the Raman spectrum at 1335 and 830 cm^{−1}.⁴³ For the azide anion, N₃[−], characteristic bands at 2092 and 1369 cm^{−1} can be observed in the infrared and Raman spectra.⁴⁴ The IR and Raman spectra of compounds **2a–b** and **7a–d** contain a set of characteristic absorption bands for the cations: 3400–3100 cm^{−1} [$\nu(\text{N–H})$], 3000–2850 [$\nu(\text{C–H})$, **7a–d**], ~1715 [$\nu(\text{C}=\text{N}5)$], 1680–1550 [$\delta(\text{N}6\text{H}_2)$, $\delta(\text{N}5\text{H}_2)$], 1550–1350 [ν , tetrazole ring, $\delta_{\text{as}}(\text{CH}_3)$ **7a–d**, $\delta(\text{N}4\text{–H})$], ~1380 [$\delta(\text{CH}_3)$ **7a–d**] 1350–700 [$\nu(\text{N}1\text{–C}1\text{–N}4)$, $\nu(\text{N–N})$, $\omega(\text{N}1\text{–N}6\text{H}_2)$ **2a–b** and **7a–d**, $\gamma(\text{CN})$, δ , tetrazole ring], <700 [δ , out-of-plane bend (N–H), $\omega(\text{N}5\text{H}_2)$]. The $\nu(\text{NH})$ absorption bands in the IR spectra of crystalline compounds **2a–b** and **7a–d** have a complex shape depending on the mode of sample preparation. In the 3100–3400 cm^{−1} region, crystalline samples show several main absorption peaks that can be assigned to N–H bonds. Because of the formation of intermolecular hydrogen bonds in the crystalline network, a red shift of the stretching modes establishes that the heteromolecular hydrogen-bond interaction between the N–H (donor) groups of the tetrazole moieties and the anion (acceptor) are strong (an increase from 25 to 40 cm^{−1} in the NH₂ asymmetric stretching area was observed). In the case of the MeDAT⁺ salts, these bands coalesce into two broad bands having a complex shape (Figure 2). To elucidate the nature of these bands, we recorded the spectra of compounds **2a–b** and **7a–d** in MeCN solutions. As an example, Figure 2 shows the solution spectra of the MeDAT⁺ salts **7a–d**. With the help of DFT calculations (Table 3), we were able to assign the stretching motions. The positions of the absorption maxima and their intensity ratio changes significantly, indicating the strong contribution of intermolecular hydrogen bonds. The spectra of **7a–d** obtained in solution are identical. The bands at 3342 (ν_1), 3213 (ν_4), 3172 (ν_3), and 3142 (ν_5) cm^{−1} were assigned to $\nu_{\text{asym}}(\text{N}5\text{H}_2)$, $\nu_{\text{asym}}(\text{N}6\text{H}_2)$, $\nu_{\text{sym}}(\text{N}5\text{H}_2)$, and $\nu_{\text{sym}}(\text{N}6\text{H}_2)$, respectively, and the band at 3262 (ν_{ob}) cm^{−1} was assigned to the binary overtone of the $\delta(\text{N}6\text{H}_2)$ (ν_6).

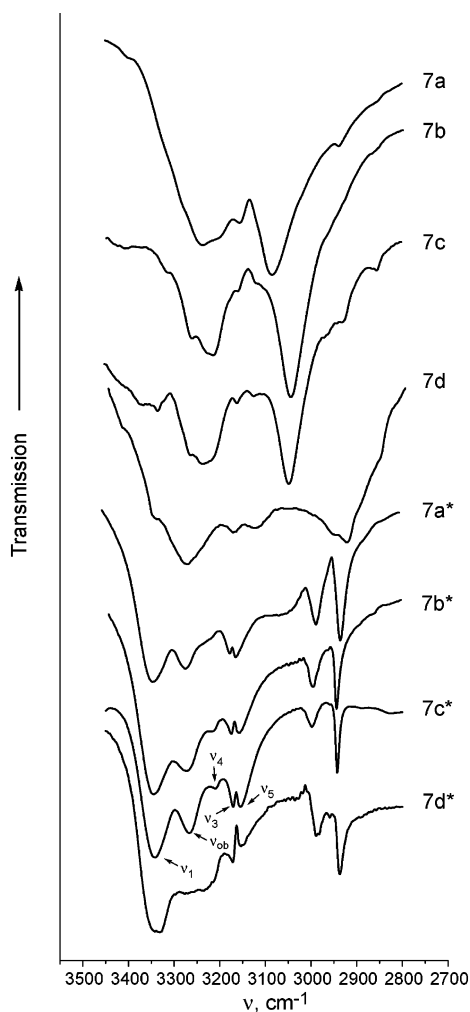
The bands observed in the spectra of crystalline samples but absent in the spectra of dilute solutions should be attributed to N–H bonds involved in intermolecular hydrogen

(37) Milcent, R.; Redeuilh, C. *J. Heterocycl. Chem.* **1980**, *17*, 1691.(38) Haussen, L. D.; Baca, E. J.; Scheiner, P. *J. Heterocycl. Chem.* **1970**, *7*, 991.(39) Drake, G.; Hawkins, T.; Brand, A.; Hall, L.; McKay, M. *Propellants, Explos., Pyrotech.* **2003**, *28* (4), 174.(40) (a) Welton, T. *Chem. Rev.* **1999**, *99*, 2071. (b) Wasserscheid, P.; Keim, W. *Angew. Chem., Int. Ed.* **2000**, *112*, 3926. (c) Wilkes, J. S. *Green Chem.* **2002**, *4*, 73.(41) (a) Williamson, K.; Li, P.; Devlin, J. P. *J. Chem. Phys.* **1968**, *48*, 3891. (b) Fernandes, J. R.; Ganguly, S.; Rao, C. N. R. *Spectrochim. Acta* **1979**, *35A*, 1013.(42) (a) Cohn, H. *J. Chem. Soc.* **1952**, 4282. (b) Redlich, P.; Holt, J.; Biegeleisen, T. *J. Am. Chem. Soc.* **1944**, *66*, 13. (c) Grothe, H.; Willner, H. *Angew. Chem., Int. Ed. Engl.* **1996**, *108*, 816.(43) Christie, K. O.; Wilson, W. W.; Petrie, M. A.; Michels, H. H.; Bottaro, J. C.; Gilardi, R. *Inorg. Chem.* **1996**, *35*, 5068.(44) Müller, U. *Struct. Bonding* **1974**, *14*, 141.

Table 3. Calculated and Experimental IR and Raman Data for **2**, **2a**, and **7a**

	approximate assignment ^b	DAT ^a	calcd ^c	IR/Raman int/act ^d	DAT ⁺ ^a	calcd ^c	IR/Raman int/act ^d	MeDAT ⁺ ^a	calcd ^c	IR/Raman int/act ^d
ν_1	$\nu_{\text{asym}}(\text{N5H}_2)$	3324/3324	3711 (3325)	67.6/40.6	3345/3363	3697 (3313)	177.5/36.8	3335/3312	3707 (3321)	143.3/28.6
ν_2	$\nu(\text{N4H})$	—	—	—	3321/3363	3625 (3248)	206.1/79.4	—	—	—
ν_3	$\nu_{\text{sym}}(\text{N5H}_2)$	3154/3193	3589 (3216)	49.2/131.8	3155/—	3561 (3191)	198.5/84.6	3216/3208	3571 (3200)	176.9/91.8
ν_4	$\nu_{\text{asym}}(\text{N6H}_2)$	3237/3243	3576 (3204)	21.3/66.3	3255/3274	3586 (3213)	65.1/50.7	3256/—	3586 (3213)	60.5/55.1
ν_5	$\nu_{\text{sym}}(\text{N6H}_2)$	3154/3154	3486 (3123)	4.4/160.2	3094/—	3488 (3125)	51.9/134.2	3105/—	3488 (3125)	48.8/151.2
ν_6	$\delta(\text{N6H}_2)$	1656/1670	1713 (1669)	154.9/8.2	1617	1686 (1643)	50.6/8.8	1614/1634	1684 (1641)	63.2/11.4
ν_7	$\nu(\text{C1-N5}) + \delta_{\text{sym}}(\text{N6H}_2)$	1632/1623	1660 (1618)	176.1/16.0	1719	1766 (1675)	436.2/3.8	1699/1705	1755 (1710)	360.0/5.4
ν_8	$\delta(\text{N5H}_2)$	—/1547	1589 (1548)	7.5/9.3	1565	1612 (1571)	19.9/4.9	1584/1607	1607 (1566)	30.1/4.7

^a Observed IR (in solution) and Raman (in the solid state) spectra, frequency in cm^{-1} . ^b Assignments are tentative because of interference from intermolecular hydrogen bonds and lattice vibrations. ^c Frequencies (cm^{-1}) calculated at the B3LYP/6-31+G(d) level. Frequencies involving mainly stretching motions of N–H groups were scaled by an empirical factor of 0.8961; in the case of bending vibrations of the NH_2 groups, a scaling factor of 0.9745 was used to maximize the agreement with the observed values. Scaled values are given in parentheses. ^d Calculated infrared intensities (km/mol) and Raman activities ($\text{\AA}^4/\text{amu}$) obtained from the B3LYP/6-31+G(d) calculations.

**Figure 2.** Spectra of **7a–d** recorded in KBr and in CH_3CN solution (*).

bonding and those not involved in intramolecular N–H bonding. Comparing the IR and Raman data of **2** with those of the corresponding protonated or methylated salts (e.g., **2a** and **7b**), some interesting results can be derived.

Table 3 reports the values obtained for these derivatives in solution (IR) and in the solid state (Raman) compared to the calculated values. The scaled calculated frequencies agree well with the experimental data. In the case of protonation (methylation), a new band can be observed at $\sim 1715 \text{ cm}^{-1}$ (**2a**) or 1699 cm^{-1} (**7a**). It can be assigned to the strongly

coupled mode (ν_7) between $\nu(\text{C1-N5})$ (ν_8) and $\delta(\text{N6H}_2)$ (ν_6) and appears at significantly higher wavenumber. The spectroscopic results are in accordance with a shortening of the C1–N5 bond and with a shorter bond length observed in the DAT salts [e.g., $1.302(4) \text{ \AA}$, **2a**] as compared to the parent compound **2** [$1.334(4) \text{ \AA}$].⁴⁵ These spectroscopic results are in excellent correlation with the crystallographic data (Table 2).

¹⁵N Chemical Shifts and ¹H–¹⁵N Coupling Constants.

In the case of **2**, the assignment of the resonances was straightforward. The ¹⁵N peaks of the amino substituents are well separated from those of the tetrazole ring. The nitrogen with the bonded amino group (N1) is the one with the most pyrrole-like character, and its NMR signal is expected to appear at highest field compared to the signals of the other nitrogen atoms.⁴⁶ The ¹⁵N{¹H} NMR spectrum of DAT shows six signals for the six different nitrogen atoms. The signals of the NH_2 groups appear as expected at high field and are strong and positive⁴⁷ when the spectrum is recorded with broadband decoupling. This is due to the strong positive nuclear Overhauser effect (NOE), resulting from the directly bonded protons. With increasing nitrogen–proton distance, the NOE changes its sign and causes a decrease of signal intensity. The dependency of the signal intensity on the NOE can thus be nicely used to assign the ¹⁵N signals in the tetrazole ring (Figure 3) and to differentiate between two- and three-coordinated nitrogen atoms, as well as between the substituted and nonsubstituted nitrogen atoms. The assignment of the peaks between the three two-coordinated nitrogen atoms can be achieved mainly by the facts that N4 has one nitrogen and one carbon as nearest neighbors, whereas N2 and N3 are surrounded by nitrogen atoms. Therefore, the signals of N2 and N3 appear at lowest field owing to electronegativity effects. This is consistent with the trends observed for other comparable ¹⁵N chemical

(45) Lyakhov, A. S.; Gaponik, P. N.; Voitekhovich, S. V. *Acta Crystallogr.* **2001**, C57, 185.

(46) (a) Markgraf, J. H.; Sadighi, J. P. *Heterocycles* **1995**, 40 (2), 583. (b) Claramunt, R. M.; Sanz, D.; López, C.; Jiménez, J. A.; Jimeno, M. L.; Elgueor, J.; Fruchier, A. *Magn. Reson. Chem.* **1997**, 35 (1), 35.

(47) (a) A. M Orendt, J. Michl. J. Reiter, *Magn. Reson. Chem.* **1989**, 27, 1. (b) N. Naulet, D. Tomé, G. J. Martin, *Magn. Reson. Chem.* **1983**, 21 (9), 564.

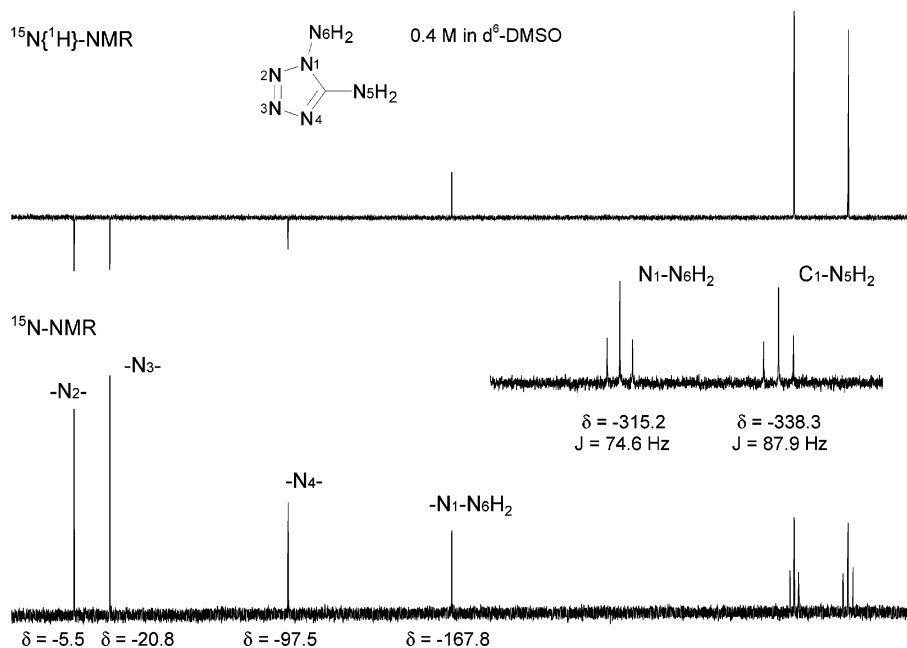


Figure 3. Proton broadband decoupled and coupled ^{15}N NMR spectra of **2** recorded in $\text{DMSO-}d_6$.

Table 4. ^{15}N and ^{13}C NMR Chemical Shifts (ppm) and Coupling Constants (J , Hz) for the Compounds Studied^a

compd ^b	N1	N2	N3	N4	N5	N6	C1 ^e
1 ^c	-137.1	-13.1	-13.1	-137.1	-338.9	—	157.2 ^c
HATNO ₃ ^{c,f}	-165.2 (-28.1)	-24.5 (11.4)	-24.5 (-11.4)	-165.2 (-28.1)	-329.1 (9.8)	—	152.4 ^c
2 ^c	-167.0	-5.5	-20.8	-97.5	-338.3	-315.2	155.0 ^c
	² J 2.3				¹ J 87.9	¹ J 74.6	
2a ^d	-164.9 (2.1)	-21.9 (-16.4)	-33.1 (-12.3)	-170.4 (-72.9)	-333.3 (5.0)	-319.6 (-4.4)	152.8, ^c 151.2 ^d
2b ^d	-169.4 (-2.4)	-20.5 (-15.0)	-36.6 (-15.8)	-177.5 (-80.0)	-329.6 (8.7)	-317.9 (-2.7)	149.7 ^d
7a ^c	-167.9 (-0.9)	-24.0 (-18.5)	-35.3 (-14.5)	-186.0 (-88.5)	-319.0 (19.3)	-307.3 (7.9)	148.1 ^c
	² J 1.7		³ J 1.9	² J 2.0		¹ J 76.1	
7d ^c	-167.9 (-0.9)	-24.3 (-18.8)	-35.9 (-15.1)	-186.7 (-89.2)	-316.8 (21.5)	-308.8 (6.4)	147.5 ^d
	² J 1.8			² J 2.0		¹ J 76.8	

^a PIS effect in parentheses. ^b All shifts were measured with respect to CH_3NO_2 internal standard; negative shifts are upfield from CH_3NO_2 . ^c $\text{DMSO-}d_6$. ^d CD_3OD . ^e ^{13}C NMR shift; ^f 5-Amino-1*H*-tetrazolium nitrate.

shifts.⁴⁸ The assignment of the N2 and N3 peaks can be achieved because of the α effect of the NH_2 group at N1. The electronegativity effect at N3 is lower than that at N2, resulting in a low-field NMR signal for N2. In the proton-coupled ^{15}N NMR spectra, where the NOE is negligible small because of the pulse delay (3 s), all ^{15}N NMR signals are positive. The $^1J(\text{H}-^{15}\text{N})$ couplings for the signals of the NH_2 groups are clearly observed, yielding triplets with coupling constants of 74.6 Hz (N6) and 87.9 Hz (N5), respectively.

The ^{15}N NMR chemical shift data of the neutral and protonated compounds are presented in Table 4. The ^{15}N protonation-induced shift (PIS) (methylation-induced for **7a** and **7d**) shows that, in $\text{DMSO-}d_6$ (CD_3OD), in all cases, the protonated form displaces the same type of cations: protonation takes place at N4 of the ring.

The greatest PIS effect is observed for N4 and is negative. In the case of the methylated derivatives **7a,d**, an upfield shift of -89.2 ppm is observed. Protonation (methylation) of the azoles increases the electron demand of the ring, favoring the perpendicular conformation of the amino group

(N5) attached to the carbon atom (C1) of the tetrazole moiety. In this way, the amino lone pair can best interact with the azolium ring. In all cases, the “PIS” effect for N5 is positive. This observation is in agreement with other relevant studies, the two most significant of which reported the use of ^{15}N NMR spectroscopy for the determination of the protonation site of *C*-aminopyrazoles⁴⁹ and *C*-amino-1,2,4-triazoles.⁵⁰ Because of fast proton exchange on the NMR time scale, only in the case of **2** and **7a** could $J(\text{H}-^{15}\text{N})$ couplings be observed.

^1H and ^{13}C NMR Spectra. In the ^1H NMR spectrum, for the resonance of the N–H-bound protons, only one signal was observed in the cases of the protonated DAT derivatives **2a** and **2b**. Compared to the starting material DAT (**2**), this signal is shifted upfield due to fast proton exchange. In the cases of the methylated derivatives for the iodide **7a** and the azide **7d**, two singlets could be observed, whereas in the cases of the nitrate **7b** and dinitramide **7c**, only one singlet was detected. Upon alkylation or protonation, a slight upfield shift is observed for the ^{13}C NMR resonances (Table 4). This

(48) Stefaniak, L.; Roberts, J. D.; Witanowski, M.; Webb, G. A. *Org. Magn. Reson.* **1984**, *22*, 209.

(49) Garrone, A.; Fruttero, R.; Tironi, C.; Gasco, A. *J. Chem. Soc., Perkin Trans. 2* **1989**, 1941.

(50) Fritz, H. *Bull. Soc. Chim. Belg.* **1984**, *93*, 559.

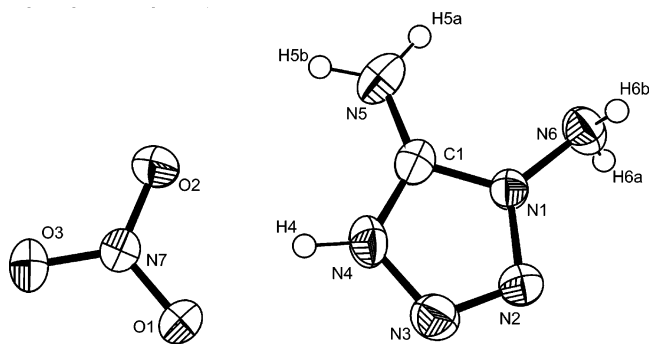


Figure 4. Formula unit and labeling scheme for 1,5-diamino-1H-tetrazolium nitrate (**2a**) (ORTEP plot, thermal ellipsoids represent 50% probability).

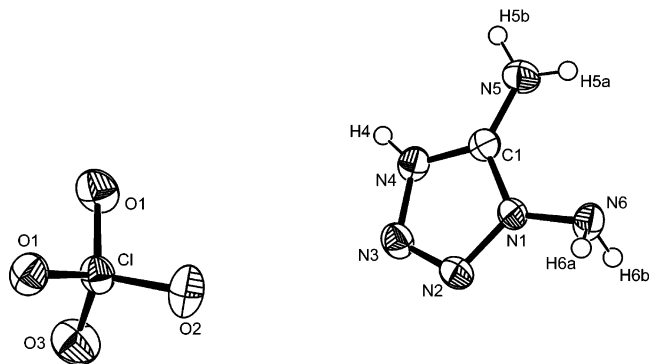


Figure 5. Formula unit and labeling scheme for 1,5-diamino-1H-tetrazolium perchlorate (**2b**) (ORTEP plot, thermal ellipsoids represent 50% probability).

effect has been observed in several other nitrogen heterocycles upon protonation or alkylation of the heterocyclic ring system.⁵¹

Crystal and Molecular Structures of 1,5-Diamino-1H-tetrazolium Salts 2a and 2b and 1,5-Diamino-4-methyl-1H-tetrazolium Salts 7b and 7d. Figures 4 and 5 show the molecular units of **2a** and **2b** with the atom labeling scheme. Selected bond lengths and angles are presented in Table 2. In accordance with other X-ray structure determinations, the DATH⁺ cations in **2a** and **2b** also have the structure in which the N4 atom is protonated (Scheme 3). The two salts, **2a** and **2b**, have as common features the molecular structure of the DATH⁺ moiety and its relative disposition with respect to the nitrate or perchlorate anion.

The DATH⁺ cations are not different, within the limits of accuracy.²⁷ The tetrazole ring is planar, with the attached exocyclic nitrogen atoms lying within this plane (the maximum deviation of N6 from this plane is 0.046 Å for **2a** and 0.074 Å for **2b**). The amino group attached to N1 is pyramidal and adopts a staggered conformation with respect to N2, similar to that observed for the unprotonated **2**.⁴⁴ This observation is consistent with a theoretical study concerning the hybridization and conformation of amino groups in *N*-aminoazoles by Foces-Foces et al. They found that sp³ hybridization of the amino groups is favored over sp² and that the amino lone pair adopts an eclipsed position with

respect to the ring in monocyclic *N*-aminoazoles, including 1-amino-1H-tetrazoles.⁵² The amino group attached to C1 is planar and lies in the plane of the tetrazole moiety (sum of angles = 360°), indicating a strong interaction of the nitrogen lone pair with the π system of the tetrazole ring. This is consistent with the observation of a shorter C1–N5 bond found for the salts compared to the parent compound **2** (Table 2). Interestingly, for unprotonated amino-*C*-azoles, e.g., 4-aminopyrazoles, two polymorphic forms are reported.⁵³ The main difference consists of the conformation of the NH₂ group with respect to the pyrazole ring: an almost eclipsed form and a twisted form are found. For **2** and for the DATH⁺ cation, a strong π-delocalization in the N1–C5–N4 fragment is found. The bond distances indicate discrete single and double bonds for the rest of the ring (Table 2). A closer inspection of the lengths of the exocyclic bonds of the amino groups to the bonded atoms [C1–N5, 1.302(4) Å (**2a**) and 1.304 Å (**2b**); N1–N6, 1.385(2) Å (**2a**) and 1.387(2) Å (**2b**)] compared to the experimental N–N and C–N distances in HN=NH and H₂N–NH₂ (1.252 and 1.449 Å, respectively) and H₂C=NH and CH₃–NH₂ (1.273 and 1.471 Å, respectively) further supports this observation⁵⁴ and displays the “hydrazinic” character of the amino group in the 1-position compared to the “aniline-like” character of the 5-amino group. The bond distances and angles in the perchlorate and nitrate anion are as observed for many other salts of nitrous or perchloric acids with amines and are omitted from Table 2.^{55,56}

In Figures 6 and 7, the molecular units of **7b** and **7d** are displayed. In the salts, the formal exchange of the proton at N4 by a methyl group shows only slight differences in the molecular parameters found for the MeDAT⁺ cation as compared to the HDAT⁺ cation. Selected bond lengths and angles are listed in Table 2. The above discussion for **2a** and **2b** also accounts for the MeDAT⁺ salts, as the methyl group hardly influences the molecular parameters. In all salts, the bond distances and angles in the five-membered ring reflect the effect of protonation, giving rise to an almost symmetrical ring with respect to an axis through C1 and the midpoint of the N2–N3 bond. The small differences in the bond lengths and angles within the cations of the salts might be the result of packing effects in the crystals.

2a crystallizes in the monoclinic space group *C2/c* with eight formula units per unit cell. The nitrate **7b** crystallizes

- (52) (a) Foces-Foces, C.; Cano, F. H.; Claramunt, R. M.; Sanz, D.; Catalan, J.; Fabero, F.; Fruchier, A.; Elguero, J. *J. Chem. Soc., Perkin Trans. 2* **1990**, 237. (b) Claramunt, R. M.; Sanz, D.; Catalán, J.; Fabero, F.; Garcia, N. A.; Foces-Foces, C.; Llamas-Saiz, A. L.; Elguero, J. *J. Chem. Soc., Perkin Trans. 2* **1993**, 1687.
- (53) Infantes; L. Foces-Foces, C.; Cabildo, P.; Claramunt, R. M.; M6, O.; Yáñez, M.; Elguero, J. *Heterocycles* **1998**, *49*, 157.
- (54) Harmony, M. D.; Laurie, V. W.; Kuczkowski, R. L.; Schwedeman, R. H.; Ramsay, D. A.; Lovas, F. L.; Lafferty, W. J.; Maki, A. G. *J. Phys. Chem. Ref. Data* **1979**, *8*, 619.
- (55) (a) Asath Bahadur, S.; Rajaram, R. K.; Nethaji, M. *Acta Crystallogr.* **1991**, *C47*, 1420. (b) Wojtczak, A.; Jaskólski, M.; Kosturkiewicz, Z. *Acta Crystallogr.* **1988**, *C44*, 1779.
- (56) (a) Alfonso, M.; Wang, Y.; Stoeckli-Evans, H. *Acta Crystallogr.* **2001**, *C57*, 1184. (b) Shao, S.-C.; Zhu, D.-R.; Zhu, X.-H.; You, X.-Z.; Shanmuga Sundara Raj, S.; Fun, H.-K. *Acta Crystallogr.* **1999**, *C55*, 1412.

(51) Sveshnikov, N. N.; Nelson, J. H. *Magn. Reson. Chem.* **1997**, *35* (3), 209.

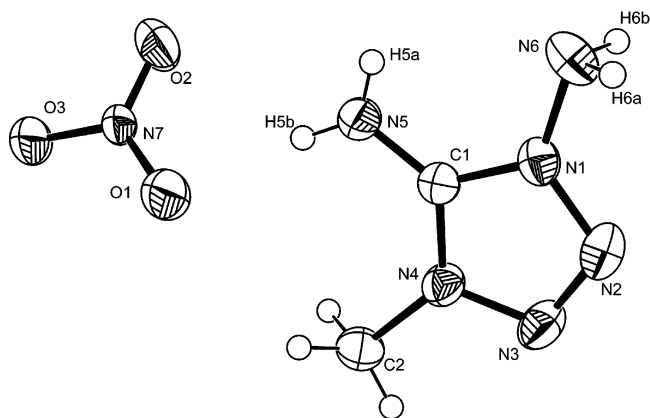


Figure 6. Formula unit and labeling scheme for 1,5-diamino-4-methyl-1*H*-tetrazolium nitrate (**7b**) (ORTEP plot, thermal ellipsoids represent 50% probability).

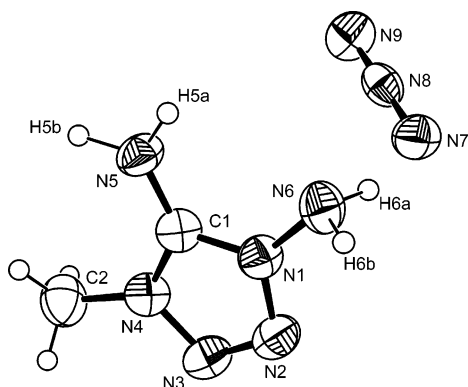


Figure 7. Formula unit and labeling scheme for 1,5-diamino-4-methyl-1*H*-tetrazolium azide (**7c**) (ORTEP plot, thermal ellipsoids represent 50% probability).

in the orthorhombic space group *Fdd2* with 16 formula units per unit cell. X-ray analysis of these two compounds confirmed that the ratio of acid to base is 1:1 and that the ions are connected through several kinds of hydrogen bonds (Table 5). Analysis of the crystal packing of **2a** and **7b** showed the existence of numerous hydrogen bonds, such as strong [e.g., $N4-H4\cdots O1 = 2.721(4)$ Å for **2a**, $N5-H5b\cdots O1 = 2.853(4)$ Å for **7b**; Table 5] and medium $N-H\cdots O$ contacts that are well within the sum of the van der Waals radii [$r_{A(O)} + r_{D(N)} = 3.10$ Å].⁵⁷ Also, the $N-H-O$ angles of $151(2)^\circ$ ($N4-H4-O1$, **2a**) and $173(4)^\circ$ ($N4-H4-O1$, **7b**), for example, are indicative of a strongly directional rather than purely electrostatic interaction. The hydrogen atom H4 on N4 in **2a** forms two intermolecular $N4-H4\cdots O1$ and $N4-H4\cdots O2$ hydrogen bonds with the two oxygen atoms ($O1$, $O2$) of the nitrate anion, yielding cation/anion pairs as depicted in Figure 8. The resulting graph set is characterized as $R_1^2(4)$, and together with the graph set $R_2^2(6)$, this module can be seen as the first-order network. The cations are linked over hydrogen bonds $N5-H5b\cdots O2^i$ and $N6-H6b\cdots O1^{ii}$ [symmetry codes: (i) $2 - x, -y, 1 - z$; (ii) $x, 1 - y, -0.5 + z$] to infinite chains that are characterized as a $C_2^2(8)$ graph set. Together with the repeating module $R_1^2(4)/R_2^2(6)$, a three-dimensional su-

(57) Bondi, A. J. *Phys. Chem.* **1964**, *68*, 441.

Table 5. Hydrogen-Bond Geometry^a (Å, deg) of **2a**, **2b**, **7b**, and **7d**

<i>D-H</i> ⋯ <i>A</i>	<i>D-H</i>	<i>H</i> ⋯ <i>A</i>	<i>D</i> ⋯ <i>A</i>	<i>D-H</i> ⋯ <i>A</i>
2a				
$N4-H4\cdots O1$	0.860(5)	1.937(2)	2.721(4)	151(2)
$N4-H4\cdots O2$	0.860(5)	2.32(2)	3.06(2)	144.0(2)
$N5-H5a\cdots N6^b$	0.860(3)	2.64(2)	2.894(2)	98.5(2)
$N5-H5a\cdots O3^i$	0.860(3)	2.66(1)	3.057(8)	109.2(2)
$N5-H5b\cdots O2^i$	0.860(6)	2.16(1)	2.93(2)	148.3(2)
$N6-H6b\cdots O1^{ii}$	0.873(4)	2.226(3)	3.014(5)	150.1(2)
2b				
$N5-H5a\cdots N6^b$	0.852(2)	2.649(1)	2.896(2)	98.17(1)
$N5-H5a\cdots O2^{iii}$	0.852(2)	2.146(2)	2.944(4)	155.68(1)
$N5-H5b\cdots O2^{iv}$	0.882(1)	2.460(3)	3.075(4)	127.28(1)
$N5-H5b\cdots O1^v$	0.882(1)	2.210(4)	3.046(5)	157.99(1)
$N4-H4\cdots O4^{vi}$	0.786(2)	2.059(6)	2.817(8)	162.14(2)
7b				
$N5-H5b\cdots O1$	0.83(4)	2.03(4)	2.853(4)	173(4)
$N5-H5a\cdots N6^b$	0.77(4)	2.57(4)	2.895(4)	108(4)
$N5-H5a\cdots O2^{vii}$	0.77(4)	2.24(4)	2.905(4)	145(5)
$N6-H6b\cdots O3^{viii}$	0.87(4)	2.25(4)	3.039(3)	151(4)
$N6-H6a\cdots O2^{ix}$	0.95(4)	2.18(4)	3.036(4)	149(3)
7d				
$N5-H5a\cdots N6^b$	0.94(6)	2.65(6)	2.892(7)	95(4)
$N6-H6a\cdots N7$	1.04(6)	2.03(6)	3.029(7)	161(5)
$N6-H6b\cdots N7^x$	0.96(7)	2.11(7)	2.973(6)	149(6)
$N5-H5a\cdots N7^{xi}$	0.94(6)	2.00(6)	2.892(6)	159(5)
$N5-H5b\cdots N9^{xii}$	1.01(5)	1.82(6)	2.830(6)	171(5)

^a Symmetry codes for **2a**: (i) $2 - x, -y, 1 - z$; (ii) $x, 1 - y, -0.5 + z$. **2b**: (iii) $0.5 - x, -0.5 + y, 0.5 - z$; (iv) $0.5 + x, -0.5 - y, -0.5 + z$; (v) $-0.5 + x, -0.5 - y, 0.5 + z$; (vi) $1 - x, -y, 1 - z$. **7b**: (vii) $-x, -y, z$; (viii) $0.25 - x, -0.25 + y, 0.75 + z$; (ix) $-x, -y, 1 + z$. **7d**: (x) $-x, 1 - y, 0.5 + z$; (xi) $x, y, -1 + z$; (xii) $0.5 + x, 1.5 - y, -1 + z$. ^b Intramolecular hydrogen bond.

pramolecular network with a planar dimeric molecular unit as the main module is formed. [The $R_4^2(12)$ graph set as the center of this unit contains the inversion center.] This unit is already identified in diaminoguanidinium nitrate as the main two-dimensional building block (Figure 1, II). These planar units are connected through $N6-H6a\cdots O1^{ii}$ [symmetry code: (ii) $x, 1 - y, -0.5 + z$] in such a way that the planes are orientated almost perpendicular to the original unit. All contacts used for the discussion of graph-set analysis of hydrogen-bond patterns are shorter than the sum of the van der Waals radii [$r_{A(O)} + r_{D(N)} = 3.10$ Å]. There are also electrostatic interactions, which are longer than the sum of the van der Waals radii and involve weak hydrogen-bond interactions [e.g., $N5-H5a\cdots O3$ 3.361(2) Å and $N6-H6a\cdots O2$ 3.201(3) Å]. They also contribute to the three-dimensional network. There is no evidence of any aromatic $\pi-\pi$ stacking interactions. Examination of the structure with PLATON⁵⁸ shows that there are no solvent-accessible voids in the crystal structure of **2a**.

The formal exchange of the hydrogen atom at N4 by a methyl group leads to a different arrangement of the ions in the case of **7b**. The motif changes completely, and the formation of planar dimeric units is no longer observed. As expected and shown by calculations of the crystal densities of energetic materials, the introduction of a methyl group leads to lower densities because of the larger voids or unfilled space [$\rho(\mathbf{2a}) = 1.73$ g cm⁻³, $\rho(\mathbf{7b}) = 1.51$ g cm⁻³].⁵⁹ The

(58) Spek, A. L. *J. Appl. Crystallogr.* **2003**, *36*, 7.

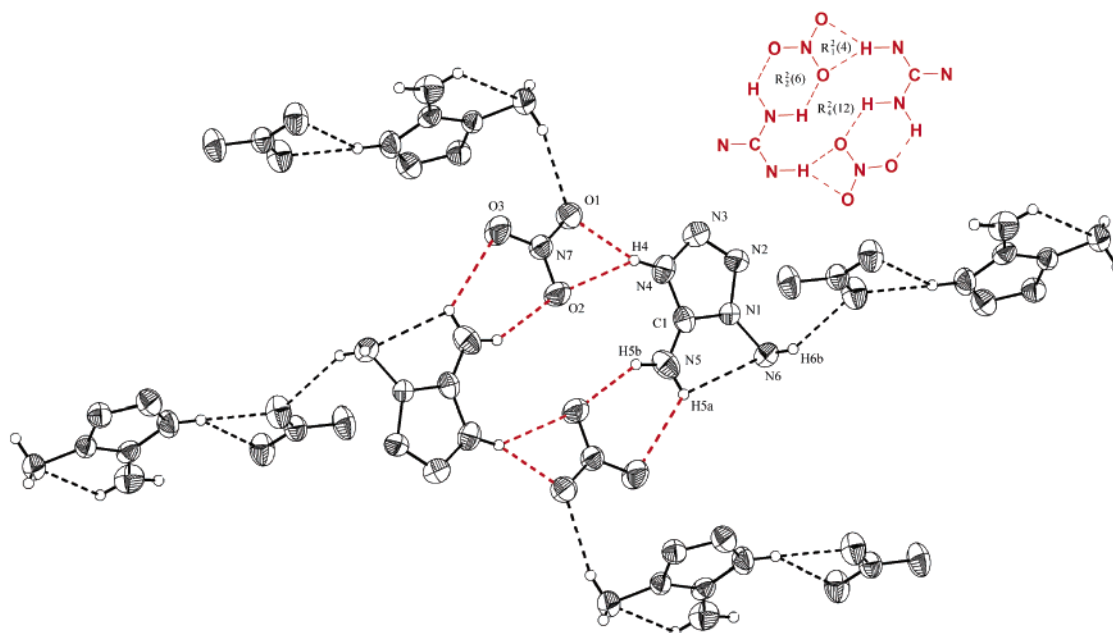


Figure 8. Surroundings of the NO_3^- anion in the structure of **2a** with hydrogen bonds to the cations marked as dotted lines (ORTEP plot, thermal ellipsoids represent 50% probability). Only strong hydrogen bonds are displayed.

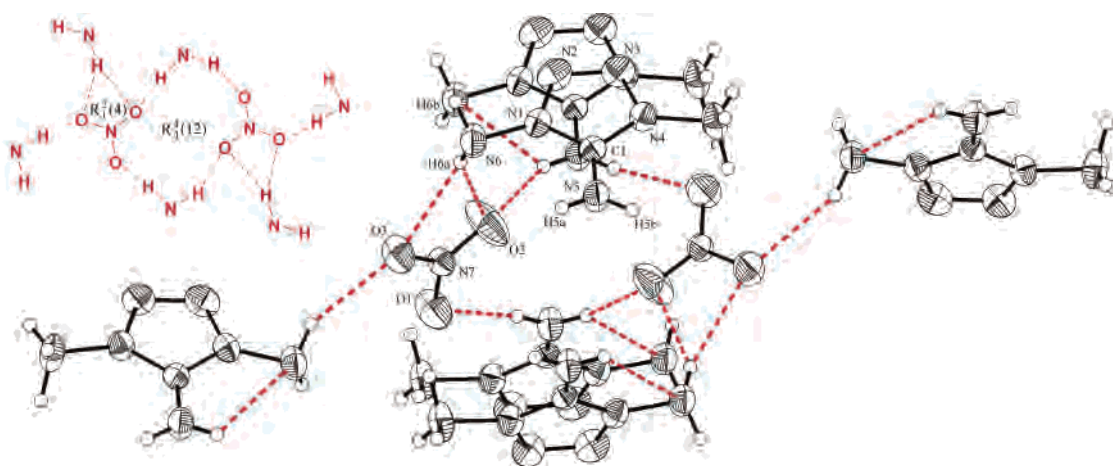


Figure 9. Surroundings of the NO_3^- anion in the structure of **7b** with hydrogen bonds to the cations marked as dotted lines (ORTEP plot, thermal ellipsoids represent 50% probability). Only strong hydrogen bonds are displayed.

replacement of the hydrogen atom in **7b** by a methyl group also leads to the formation of a three-dimensional hydrogen-bond network. However, the mismatching of donor and acceptor sites placed on the two counterions, compared to $[\text{HAGN}^+\text{NO}_3^-]$ (Figure 1, **I**) and **2b**, leads to a significantly modified crystal organization and the appearance of only two ring graph sets [$R_1^2(4)$, $R_4^4(12)$, Figure 9].

2b crystallizes in the monoclinic space group $P2_1/n$ with four formula units per unit cell. Compared to **2a**, the exchange of the counterion by the perchlorate ion in the case of **2b** also leads to the formation of dimeric subunits [the $R_4^2(8)$ graph set as the center of this unit contains the inversion center], but because of the symmetry of the perchlorate anion (T_d), these units do not lie in one plane

(Figure 10). Interestingly, the main graph-set subunit of **2a** [$R_4^2(12)$] is reduced in **2b** to $R_4^2(8)$, which can be understood by the formal decrease of the bond angle at the central atom of the anion from 120° in the NO_3^- anion to 109° in the perchlorate anion. Within the crystal structure of **2b**, only O1, O2, and O4 of the perchlorate anion are involved in hydrogen-bond interactions; the shortest interaction of O3 (O3–N4) is $3.321(2)$ Å without any hydrogen-bond interaction. Therefore, because of the formal symmetry change of the ClO_4 moiety (tetrahedral) compared to the NO_3 anion (planar), the reduction of the symmetry leads to a modified crystal organization and the observation of a new graph set [$R_4^2(8)$].

The X-ray crystal structure of **7d** (orthorhombic, space group $Pna2_1$, Figure 11) reveals that the azide anion links the cations over four strong hydrogen bridges (Table 5) in such a way that N7 forms three hydrogen bridges, i.e., N6–

(59) (a) Piacenza, G.; Legsai, G.; Blaive, B.; Gallo, R. *J. Phys. Org. Chem.* **1996**, *9*, 427. (b) Immirzi, A.; Perini, B. *Acta Crystallogr.* **1977**, *A33*, 136. (c) Ammon, L.; Mitchel, S. *Propellants, Explos., Pyrotech.* **1998**, *23* (4), 260.

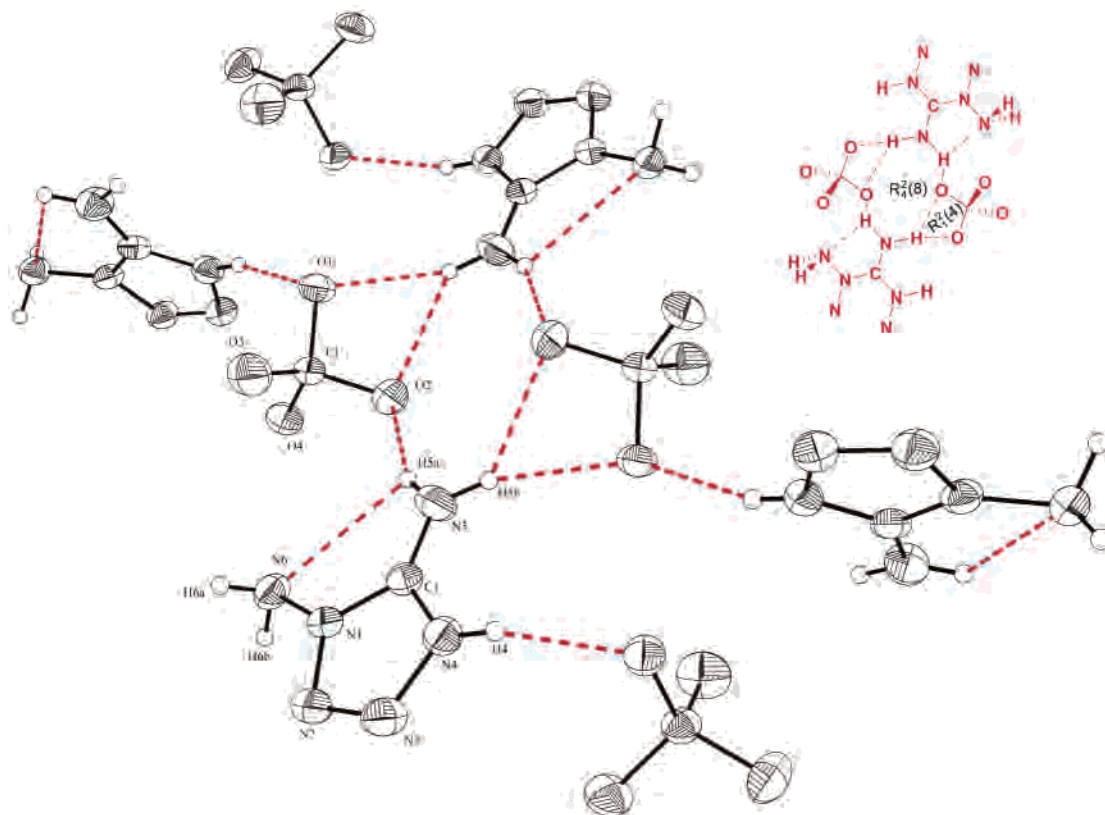


Figure 10. Surroundings of the ClO_4^- anion in the structure of **2b** with hydrogen bonds to the cations marked as dotted lines (ORTEP plot, thermal ellipsoids represent 50% probability). Only strong hydrogen bonds are displayed.

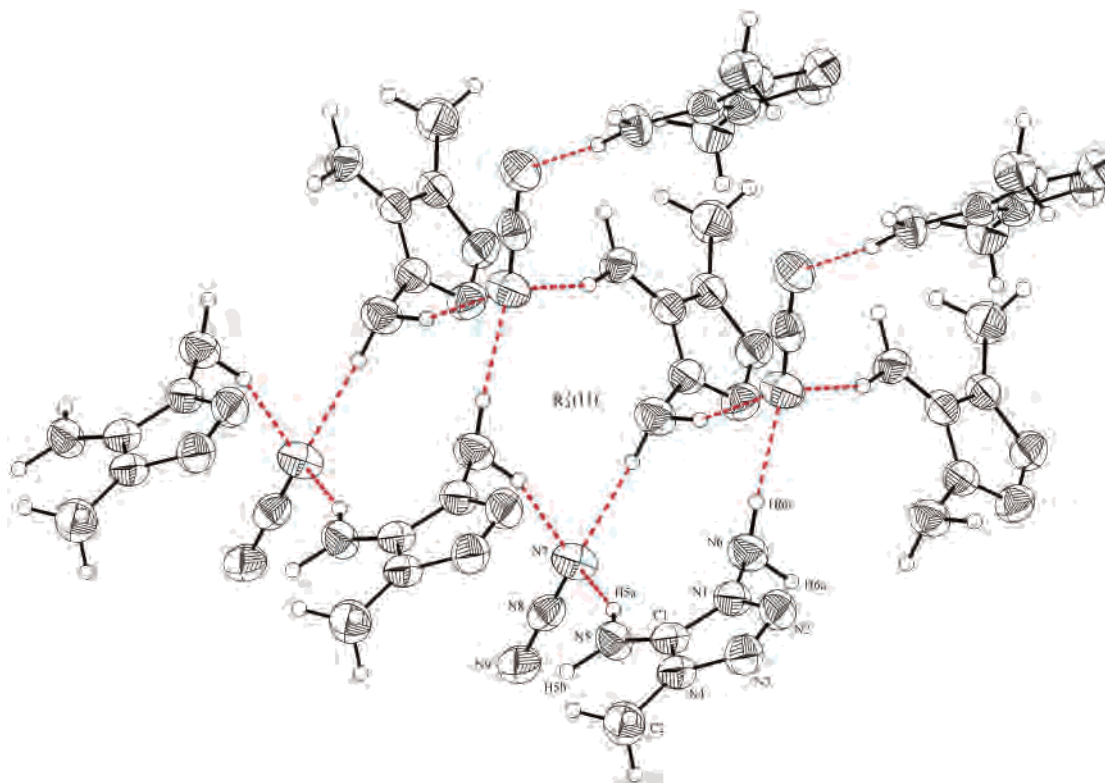


Figure 11. Surroundings of the N_3^- anion in the structure of **7d** with hydrogen bonds to the cations marked as dotted lines (ORTEP plot, thermal ellipsoids represent 50% probability). Only strong hydrogen bonds are displayed. The intramolecular hydrogen bond is omitted for clarity.

$\text{H6a} \cdots \text{N7}$, $\text{N6} - \text{H6b} \cdots \text{N7}^x$, and $\text{N5} - \text{H5a} \cdots \text{N7}^{\text{xi}}$ [symmetry codes: (x) $-x, 1 - y, 0.5 + z$; (xi) $x, y, -1 + z$] whereas N9 forms only one, i.e., $\text{N5} - \text{H5b} \cdots \text{N9}^{\text{xii}}$ [symmetry codes:

(xii) $0.5 + x, 1.5 - y, -1 + z$]. The different coordination patterns of the terminal nitrogen atoms of the azide group explain the observed difference in the $\text{N7} - \text{N8}$ [1.184(5) Å]

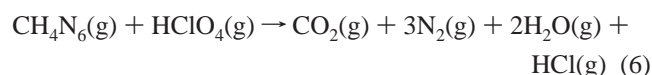
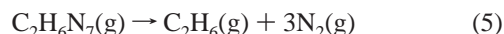
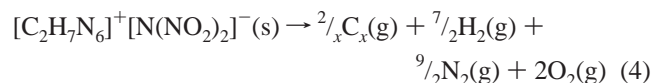
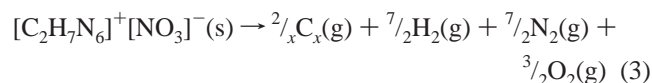
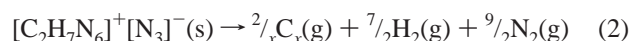
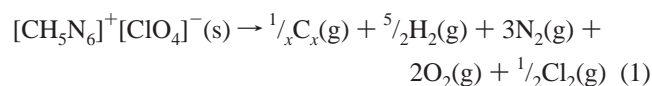
Table 6. Thermochemical Results for the Synthesized Salts **2a**, **2b**, and **7b–d**

	abcdef ^a	Ω^b (%)	ρ^c (g/cm ³)	$\Delta_f H^d$	$\Delta_c H_{\text{calcd}}^e$	$\Delta_f H_{\text{calcd}}^f$	$\Delta_c U_{\text{exp}}^g$	$\Delta_c H_{\text{exp}}^h$	T_m^i	T_d^j
2a ⁱ	156103	-14.7	1.727	+60.7	-1993	-1245	-311	-1888	138	168
2b	156014	-5.5	1.902	+45.9 (+40.4)	-1036	-928	-199	-972	97	192
7b	276103	-40.6	1.506	+41.7 (+41.2)	-2645	-1039	-439	-2456	121	181
7c	276304	-25.3	1.719	+92.1 (+91.1)	-2346	-1179	-478	-2135	85	184
7d	276300	-76.4	1.417	+161.6 (+161.5)	-3744	-1028	-570	-3594	135	137

^a Encoded formula. ^b Oxygen balance. ^c Calculated density from X-ray structure. ^d Calculated molar enthalpy of formation in kcal mol⁻¹ using G2 (G3) method. ^e Calculated molar enthalpy of combustion in cal g⁻¹. ^f Calculated molar enthalpy of detonation in cal g⁻¹. ^g Experimental constant-volume combustion energy in kcal mol⁻¹. ^h Experimental molar enthalpy of combustion in cal g⁻¹. ⁱ From DSC experiments ($\beta = 10$ °C min⁻¹); T_m , melting point; T_d , peak maximum temperature of the decomposition step (°C). ^j From ref 14c.

and N8–N9 [1.170(5) Å] bond lengths. The observed distances for NH...N hydrogen bonds agree well with the distances found in other ionic azide compounds.^{19,20} A rather unusual graph set [$R_4^2(11)$] is found for **7d**. These motifs are connected in such a fashion through a 2-folded axis, that infinite chains are formed. Together with the hydrogen bond N5–H5b...N9^{xii}, these chains are connected to a three-dimensional network.

Thermodynamic Aspects. The heats of combustion for compounds **2b** and **7b–7d** were determined experimentally and are summarized in Table 6. The enthalpies of formation for the salts **2b** and **7b–7d** were calculated by following the Born–Haber energy cycles^{14c,60} (Scheme 7) according to reactions 1–4. The reaction enthalpies ($\Delta_R H$) for reactions 5 and 6 were calculated using the parametrized ab initio molecular orbital methods Gaussian-2 (G2)⁶¹ and Gaussian-3 (G3).⁶²



From the computed G2 and G3 enthalpies (Table S1, Supporting Information), the reaction enthalpy $\Delta_R H$ for

reaction 5 was calculated to be -125.4 (G2) and -125.0 (G3) kcal mol⁻¹, and that for reaction 6 was found to be -341.1 (G2) and -335.4 (G3) kcal mol⁻¹.

The corresponding lattice enthalpies, ΔH_L , for salts M_pX_q were derived from U_{POT} using the relationship provided by Jenkins et al. (eq A)

$$\Delta H_L = U_{\text{POT}} + [p(n_M/2 - 2) + q(n_X/2 - 2)]RT \quad (\text{A})$$

where n_M and n_X depend on the nature of the ions M^{p+} and X^{q-} , respectively, and are equal to 3 for monatomic ions, 5 for linear polyatomic ions, and 6 for nonlinear polyatomic ions.⁶³ The equation for lattice potential energy U_{POT} (eq B) has the form

$$U_{\text{POT}} (\text{kJ mol}^{-1}) = 2I[\alpha(V_m)^{-1/3} + \beta] \quad (\text{B})$$

where $\alpha = 117.3$ and $\beta = 51.9$ according to the stoichiometries of the salts **2b** and **7b–7d** [M_pX_q ; $p = p = 1$; $I = \frac{1}{2}(pq^2 - qp^2) = 1$]. V_m is the molecular volume ($V_m = V/Z$). With the calculated enthalpies of reactions 5 and 6 and the experimentally known enthalpies of formation for $\text{HNO}_3(\text{g})$, $\text{HN}_3(\text{g})$, $\text{HN}(\text{NO}_2)_2(\text{g}, \text{calcd})$,⁶⁴ $\text{C}_2\text{H}_6(\text{g})$, $\text{CH}_4(\text{g})$, and $\text{N}_2(\text{g})$ [$\Delta_f H^\circ$ (exp), Table S1 (Supporting Information)] and proton affinities (P_A , Table S1), also calculated with G2 and G3 methods, it was possible to calculate the standard enthalpies of formation for the salts **2b** and **7b–7d**. Using the so-obtained values for the enthalpies of formation and the literature values for the enthalpies of formation of $\text{H}_2\text{O}(\text{l})$ [$\Delta_f H^\circ(\text{H}_2\text{O}) = -68.1$ kcal mol⁻¹],^{65,66} $\text{CO}_2(\text{g})$ [$\Delta_f H^\circ(\text{CO}_2) = -94.2$ kcal mol⁻¹],⁶⁷ and $\text{HCl}(\text{g})$ [$\Delta_f H^\circ(\text{HCl}) = -22.3$ kcal mol⁻¹],⁶⁶ it was also possible to calculate the enthalpies

(60) Klapotke, T. M.; Rienacker, C. M.; Zewen, H. Z. *Anorg. Allg. Chem.* **2002**, 628, 2372.

(61) (a) Curtis, L. A.; Head-Gordon, M.; Fox, D. J.; Ragahavachari, K.; Pople, J. A. *J. Chem. Phys.* **1989**, 90, 5622. (b) Curtiss, L. A.; Ragahavachari, K.; Trucks, G. W.; Pople, J. A. *J. Chem. Phys.* **1991**, 94, 7221. (c) Curtiss, L. A.; Ragahavachari, K.; Redfern, P. C.; Pople, J. A. *J. Chem. Phys.* **1998**, 109, 42.

(62) Curtiss, L. A.; Ragahavachari, K.; Redfern, P. C.; Pople, J. A. *J. Chem. Phys.* **1998**, 109, 7764.

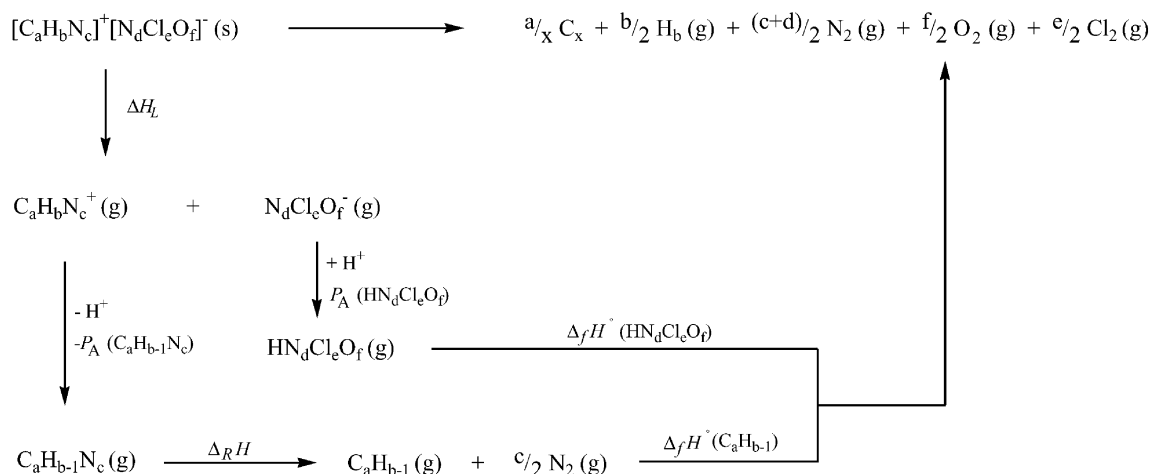
(63) Jenkins, H. D. B.; Tudeal, D.; Glasser, L. *Inorg. Chem.* **2002**, 41 (9), 2364.

(64) Michels, H. H.; Montgomery, J. A., Jr. *J. Phys. Chem.* **1993**, 97, 6602.

(65) *NIST Chemistry WebBook; NIST Standard Reference Database Number 69*; National Institute of Standards and Technology (NIST): Gaithersburg, MD, Mar 2003; <http://webbook.nist.gov/chemistry/>.

(66) Cox, J. D.; Wagman, D. D.; Medvedev, V. A. *CODATA Key Values for Thermodynamics*; Hemisphere Publishing Corp.: New York, 1984; p 1.

(67) Chase, M. W., Jr. *NIST-JANAF Thermochemical Tables*, 4th ed.; Chase, M. W., Jr., Ed.; American Chemical Society: Washington, D.C., 1998.

Scheme 7. General Born–Haber Energy Cycle for the Reactions 1–4^a

^a For encoding of compounds **2a**, **2b**, and **7b–d**, see Table 6.

of the (oxygen) combustion of the salts **2b** and **7b–7d** according reactions 7–10.

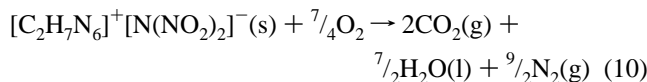
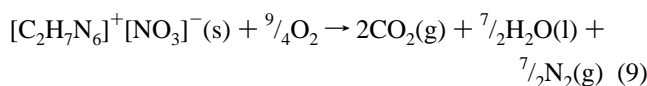
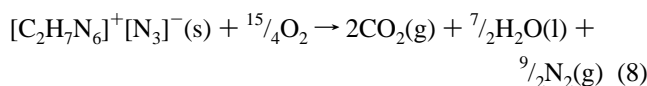
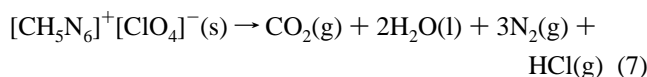
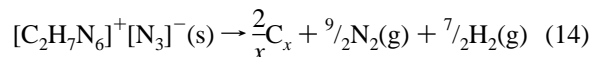
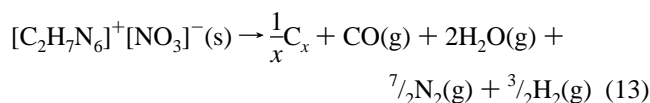
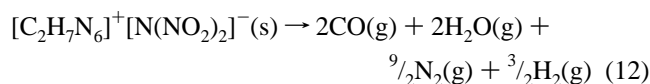
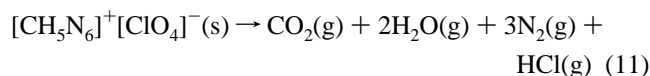


Table S1 (Supporting Information) summarizes the thermochemical and structural data needed for the calculations of the heats of formation of compounds **2b** and **7b–7d**. Table 6 shows a comparison of the experimentally determined (see Experimental Section) and calculated heats of combustion (on the basis of the Born–Haber energy cycles; see Scheme 7) for the salts **2b** and **7b–7d**. Typical experimental results (averaged over three measurements each) of the constant-volume combustion energy ($\Delta_c U$) of the new salts are presented in Table 6. The standard molar enthalpies of combustion ($\Delta_c H^{\circ}$) were derived from the expression $\Delta_c H^{\circ} = \Delta_c U + \Delta nRT$ (where $\Delta n = \sum n_i(\text{products}, \text{g}) - \sum n_i(\text{reactants}, \text{g})$ and $\sum n_i$ is the total molar amount of gases in the products or reactants). The obtained values are in reasonable agreement with the experimentally determined values, with a deviation of less than 9%; for example, in the case of **7d**, $\Delta_c H^{\circ}_{\text{calcd}}$ and $\Delta_f H^{\circ}$ were found to be $-3744 \text{ kcal g}^{-1}$ and $161.6 \text{ kcal mol}^{-1}$, respectively, which is in good agreement with the experimentally obtained value of $-3594 \text{ kcal g}^{-1}$ ($\Delta_c H^{\circ}_{\text{exp}}$).

To determine the decomposition products and assess more quantitatively the expected detonation properties of the salts **2b** and **7b–7d**, the Kistiakowsky–Wilson rule for salts **2b** and **7c** (reactions 11 and 12) and the modified K–W rule

for **7b** and **7d** (reactions 13 and 14, Ω lower than -40%) were used, together with the experimentally known enthalpies of formation of $\text{H}_2\text{O}(\text{g})$ [$\Delta_f H^{\circ}(\text{H}_2\text{O}) = -57.8 \text{ kcal mol}^{-1}$],^{65,66} $\text{CO}(\text{g})$ [$\Delta_f H^{\circ}(\text{CO}) = -26.5 \text{ kcal mol}^{-1}$],⁶⁷ and $\text{HCl}(\text{g})$ [$\Delta_f H^{\circ}(\text{HCl}) = -22.3 \text{ kcal mol}^{-1}$],⁶⁶ to derive the enthalpies of detonation ($\Delta_E H^{\circ}_{\text{calcd}}$) for the salts **2b** and **7b–7d** (see Table 6).



The expected detonation pressures (P) and detonation velocities (D) were calculated using the semiempirical equations suggested by Kamlet and Jacobs (eqs C and D, Table 7).^{68–70}

$$P (10^8 \text{ Pa}) = K\rho^2\varphi \quad (C)$$

$$D (\text{mm } \mu\text{s}^{-1}) = A\varphi^{1/2}(1 + B\rho) \quad (D)$$

For compounds **2b** and **7b–7d**, the calculated detonation pressures lie in the range between $P = 20.8 \text{ GPa}$ [**7d**]; comparable to that of the explosive TNT (2,4,6-trinitrotolu-

(68) (a) Kamlet, M. J.; Jacobs, S. J. *J. Chem. Phys.* **1968**, *48*, 23. (b) Kamlet, M. J.; Ablard, J. E. *J. Chem. Phys.* **1968**, *48*, 36. (c) Kamlet, M. J.; Dickinson, C. *J. Chem. Phys.* **1968**, *48*, 43.

(69) (a) Eremanko, L. T.; Nesterenko, D. A. *Chem. Phys. Rep.* **1997**, *16*, 1675. (b) Astakhov, A. M.; Stepanov, R. S.; Babushkin, A. Y. *Combust. Explos. Shock Waves*. **1998**, *34*, 85 (Engl. Transl.).

(70) Where $K = 15.58$, ρ (g cm^{-3}), $\varphi = N\sqrt{M(-\Delta_E H)}$, N is the number of moles of gases per gram of explosives, M is the average molar mass of the formed gases, $\Delta_E H$ is the calculated enthalpy of detonation (in cal g^{-1}), $A = 1.01$, and $B = 1.30$.

Table 7. Explosive Properties and Initial Safety Testings of the Synthesized Salts **2a**, **2b**, and **7b–d**

	<i>P</i> (GPa)	<i>D</i> (m s ⁻¹)	impact ^a (kg cm) (Nm)	friction ^{b,c}
2a	33.3	8774	90 (9 J)	192 N (–)
2b	32.2	8383	70 (7 J)	60 N (+)
7b	23.4	7682	>200 (>40 J)	120 N (–)
7c	33.6	8827	70 (7 J)	24 N (+)
7d	20.8	7405	150 (15 J)	192 N (–)

^a Insensitive > 40 J, less sensitive ≥ 35 J, sensitive ≥ 4 J, very sensitive ≤ 3 J. ^b Insensitive > 360 N, less sensitive = 360 N, sensitive < 360 N and > 80 N, very sensitive ≤ 80 N, extreme sensitive ≤ 10 N. ^c According to the *UN Recommendations on the Transport of Dangerous Goods, Manual of Tests and Criteria*,^{73a} (+) indicates not safe for transport.

ene),⁷¹ for which *P* = 20.6 GPa] and *P* = 33.6 GPa (**7c**; comparable to that of the explosive RDX (hexahydro-1,3,5-trinitro-1,3,5-triazine),⁷¹ for which *P* = 34.4 GPa). Detonation velocities are in the range between *D* = 7405 m s⁻¹ (**7d**; comparable to that of nitroglycerin,⁷² *D* = 7610 m s⁻¹) and *D* = 8827 m s⁻¹ (**7c**; comparable to that of RDX,⁷² *D* = 8750 m s⁻¹). In the cases of the chloride-free salts, these values correlate well with the increase of density [**7d** (1.417) < **7b** (1.506) < **7c** (1.719) ≈ **2a** (1.727)].

Impact testing was carried out on a BAM Fallhammer in accordance with the BAM method.^{73b} A small amount of preweighed sample, usually around 20 mg, was placed in a brass cup for each test. As a standard, 6-μm HMX (high melting point explosive) was tested previously, giving value of 34 kg cm for five consecutive negative results. Drop heights were measured for the falling of 1- and 5-kg masses and a minimum drop height considered for five consecutive drops at a specific height and mass with no change in sample. From Table 7, it is obvious that there is a range in impact sensitivities, from the insensitive nitrate **7b** (>40 J) to the less sensitive azide **7d** (15 J) compared to **2a** (9 J), **2b** (7 J), and **7c** (7 J). However, in all cases, the salts are less sensitive to impact than the highly used dry explosives RDX (5 J), Tetryl (4 J), or the more sensitive pentaerythritoltetranitrate (PETN; 3 J).⁷⁴ Interestingly, the friction sensitivity of the

compounds is much higher than expected (Table 7). In the cases of the nitrates **2a** and **7b** and unexpectedly the azide **7d**, the friction sensitivity—determined with a BAM friction tester⁷⁵—lies in the sensitivity range of common secondary explosives such as RDX (dry, 120 N) or nitrocellulose (dry, 240 N). However, the highly energetic salt **2b** (60 N) should be handled with extreme care, as its friction sensitivity reaches values comparable to that of the very sensitive PETN (dry, 60 N). The dinitramide salt **7c** exhibits the highest friction sensitivity with a value of 24 N, which is still lower than that of the very sensitive lead azide (10 N).

Conclusion

The synthesis of DAT (**2**) presented herein provides a new and easier approach to the highly energetic salts **2a**, **2b**, **7b**, and **7c**. All new salts examined in this work exhibit good to reasonable physical properties, such as high densities (>1.50 g cm⁻³), good thermal stabilities, and distinctive melting points around 100 °C. Depending on their properties, these salts can be seen as new examples of secondary explosives (**2a**, **7b**, ~**7d**) or primary explosives (**7c** and **7d**). All of these compounds show calculated detonation velocities and detonation pressures comparable to those of high explosives such as PETN, RDX, and HMX. The molar enthalpies of formation of the new salts were calculated from the combustion energies obtained from corresponding oxygen bomb calorimetric measurements and in all cases show high combustion energies and high molar enthalpies of formation. From a closer inspection of the crystal structure, intermolecular hydrogen bonding is seen to play an important role in crystal packing, and together with the formalism of graph-set analysis of hydrogen-bond patterns, interesting results could be derived.

Acknowledgment. The authors are indebted to and thank Prof. Dr. P. Klüfers for his generous allocation of X-ray diffractometer time. Financial support of this work by the University of Munich (LMU) and the Fonds der Chemischen Industrie is gratefully acknowledged (J.J.W. acknowledges a FCI scholarship, DO 171/46). The authors are also indebted to and thank Mr. Gunnar Spiess for the calorimetric measurements and the drop hammer and friction tests.

Supporting Information Available: Summary of the thermochemical and structural data needed for the calculations of the heats of formation of compounds **2b** and **7b–7d** (Table S1) and crystallographic data in CIF format. This material is available free of charge via the Internet at <http://pubs.acs.org>.

IC050104G

(75) Reichel & Partner GmbH, <http://www.reichel-partner.de/>.

(71) Mader, C. L. *Detonation Properties of Condensed Explosives Computed Using the Becker–Kistiakowsky–Wilson Equation of State*; Report LA-2900; Los Alamos Scientific Laboratory: Los Alamos, NM, 1963.

(72) Köhler, J.; Mayer, R. *Explosivstoffe*, 7. Aufl.; Wiley-VCH: Weinheim, Germany, 1991.

(73) (a) Test methods according to the *UN Recommendations on the Transport of Dangerous Goods, Manual of Tests and Criteria*, 4th rev. ed.; United Nations Publication: New York, 2003. (b) 13.4.2 Test 3(a)(ii) BAM Fallhammer.

(74) WIWEB (Wehrwissenschaftliches Institut für Werk-, Explosiv- und Betriebsstoffe; Bundeswehr Research Institute for Materials, Explosives, Fuels and Lubricants), Koblenz, Germany. Private communication.